



Total Control

*Advanced integrated supervisory and wind turbine control
for optimal operation of large Wind Power Plants*

Tower load reduction with LiDAR-assisted control
& Individual Pitch Control with tower top sensors

Deliverable no. 3.5

Delivery date: (16.12.2019)

Lead beneficiary: DNV GL

Dissemination level:



This project has received funding
from the European Union's Horizon
2020 Research and Innovation
Programme under grant agreement
No. 727680

Author(s) information (alphabetical):

Name	Organisation	Email
Mattia D'Angelo	DNV GL	mattia.dangelo@dnvgl.com

Acknowledgements/Contributions:

Name	Name	Name
Ervin Bossanyi, DNV GL		

Document information

Version	Date	Description	Prepared by	Reviewed by	Approved by
1	18.12.2019		Mattia D'Angelo	Martin Evans	Ervin Bossanyi

Definitions/Abbreviations

LAC	Lidar Assisted Control
LAT	Look Ahead Time
IPC	Individual Pitch Control
TT IPC	Tower Top IPC
BR IPC	Blade Root IPC
RNA	Rotor Nacelle Assembly

TABLE OF CONTENTS

Executive summary	4
1. LiDAR Assisted Control.....	4
1.1. Wind Estimation	5
1.1.1. Modelling of DTU Spinner LiDAR in Bladed	5
1.1.2. Estimation of Rotor Average Wind Speed	6
1.1.3. Estimation Results	8
1.2. Feed Forward Algorithm	10
1.2.1. Look Ahead Time	11
1.2.2. Feed Forward Pitch Rate.....	11
1.2.3. Collective pitch-speed controller gains	12
1.3. Controller Performance	13
1.4. Fatigue Loads (DEL) Results	15
1.4.1. Load Case Definition.....	15
1.4.2. Damage equivalent loads.....	16
2. Tower Top IPC	18
2.1. Theory	18
2.2. Tower Top IPC	19
2.2.1. Spectral Analysis	23
2.2.2. Fatigue Loads (DEL) Results	25
2.3. 2P IPC	29
2.3.1. Spectral Analysis	30
2.3.2. Fatigue Loads (DEL) Results	33
3. Conclusions.....	37
4. References.....	38

EXECUTIVE SUMMARY

This report describes work carried out as part of TotalControl task 3.1.4, which is concerned with modification of the control system of the wind turbine to include Tower Top IPC and LiDAR Assisted Control (LAC) for load reduction.

Tower top IPC makes use of tower top strain gauges instead of blade root strain gauges as the measurement input, and is of interest because of the likely lower cost and higher reliability and maintainability of these gauges.

LAC makes use of wind preview information from a forward-facing nacelle-mounted LiDAR to improve the control, and has the potential to reduce fatigue loading and pitch duty.

Both control strategies have been implemented in the turbine controller, and simulations show that with LAC, lifetime damage equivalent loads in tower base fore-aft bending moment are reduced by 5.7%, while maintaining similar levels of generator speed regulation.

1P Tower top IPC closely matches the load reduction provided by the standard method using blade root sensors, while for 2P IPC, the conventional method outperforms Tower Top IPC. The results show a relative difference in hub loads reduction of 5-7% between Blade Root IPC and Tower Top IPC, but both strategies provide further reductions compared to just 1P IPC.

Both of these strategies have been implemented in the controller for the 7MW Levenmouth turbine, and tested using *Bladed* simulations, so that they are ready to be deployed on the turbine for field testing to be reported in deliverable D3.7. Since the original controller was not designed to include 2P IPC, the alarms defined in the supervisory controller should be revised to accommodate the field test.

1. LIDAR ASSISTED CONTROL

LiDAR Assisted Control uses wind preview information from a LiDAR to proactively steer the collective pitch angle towards the ideal value. In order to tune the controller, an accurate representation of the turbine and the LiDAR are needed to perform high fidelity simulations.

Section 1.1 describes the method and assumptions used to simulate the DTU SpinnerLiDAR in *Bladed* and obtain the wind speed estimates required by the feed forward algorithm described in Section 1.2.

Section 1.3 compares the performance of the LAC controller versus to the baseline, and Section 1.4 analyses the results.

1.1. Wind Estimation

1.1.1. MODELLING OF DTU SPINNER LIDAR IN BLADED

A LIDAR sensor is a laser Doppler anemometer which sends out a laser beam and detects returning reflections from small particles or aerosols moving with the wind. Through the Doppler effect, the difference in frequency between outgoing and incoming signals gives a direct measure of the reflecting particle's velocity component in the direction of the beam line. Each measured velocity sample uses reflections from many particles, distributed within a volume of air in the vicinity of the focal point.

In Bladed, this is implemented by means of a weighting function used to calculate a weighted average of actual velocities, resolved into the direction of the beam, at a series of points along the beam [1].

The weighting function for a continuous-wave LIDAR depends on the laser wavelength λ , the lens area A , and the distance R to the focal point:

$$w(x) = \frac{R^2}{(1 + c^2)} \frac{1}{(R + x)^2 + (x/c)^2}, c = R\lambda/A$$

The LiDAR that was used in this task, and that will be used for the field tests, is the DTU Spinner LiDAR, which uses a continuous-wave laser scanning the wind sequentially at 400 points along a rosette pattern at a focal distance of 150m [2]. Table 1 describes the LiDAR key parameters, and its mounting position on the turbine

Table 1 DTU Spinner LiDAR Key Parameters and mountig position

Lase type	Continuous
Number of Beams	1
Points per Scan	400
Sampling method	Sequential
Time for one complete san	1s
Max. Cone half angle	30 deg
Max. Cone half angle	0 deg
Focal distance	150m
Laser wave length, λ	1.565 nm
Laser Area, A	0.00126 m ²
$\alpha = \lambda / A$	1.2421×10^{-6}

The LiDAR is mounted on the nacelle of the Samsung 7WM turbine in Levonmouth, and mounting location reported in Table 2. This corresponds to the LiDAR being mounted about 1.5m above the nacelle roof, and 4.3m upstream of the yaw bearing centreline.

Table 2 Mounting position relative to the Yaw Bearing coordinate system

X – Location	-4.3m
Y – Location	0 m
Z - Location	8.7m

The values in Table 1 and Table 2 were used to define the LiDAR in Bladed; however, there is a difference between Bladed’s predefined rosette scanning pattern, and the Spinner LiDAR pattern, as shown in Figure 1. It is possible in Bladed to define arbitrary scanning patterns through the external controller API; however, the controller for the Samsung turbine was developed before this capability was added to Bladed, and therefore it was not possible to use the API to match the Spinner LiDAR rosette in simulation. However, both scanning patterns provide excellent coverage of the swept area, so the difference is unlikely to be important.

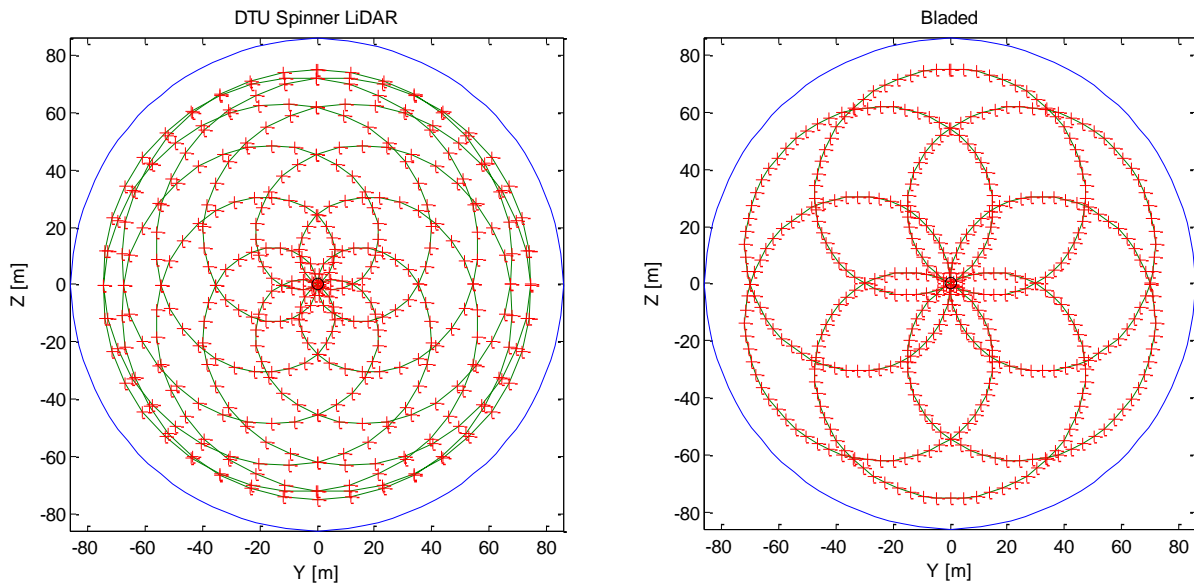


Figure 1 Difference in rosette scanning pattern between DTU Spinner LiDAR and Bladed

1.1.2.

ESTIMATION OF ROTOR AVERAGE WIND SPEED

In the field tests for task 3.2, the estimates of wind properties would be performed by the LiDAR itself and fed to the turbine controller directly for use in the feed forward control loop.

In the simulation environment, the line-of-sight measurement from the Bladed model of the LiDAR need to be converted in to estimates of the rotor-averaged quantities, such as longitudinal wind speed, wind direction and up-flow angle. The estimation can never be perfect for many reasons, notably:

- a) As the LIDAR only measures the component of wind speed along the beam, assumptions must be made to estimate the other components.
- b) The LIDAR is not sampling the whole swept area.
- c) The higher frequency parts of the measured turbulence will change by the time they reach the turbine.

For this work, the main parameter of interest is the longitudinal wind speed estimate, which is computed by the turbine controller at every controller cycle. The general method for estimating the longitudinal component consists of modelling the line-of-sight wind speed, $v_{los,i}$, of each focus point $[x_i \ y_i \ z_i]$ as the projection of the wind vector $[u_i \ v_i \ w_i]^T$ at the i th focus point onto the beam direction:

$$v_{los,i} = l_{xi}u_i + l_{yi}v_i + l_{zi}w_i \quad (1)$$

Where l_{xi} , l_{yi} , l_{zi} are the direction cosines between $\overrightarrow{v_{los,i}}$ and the wind vector. It is then assumed that no shears and inflow angles are present, $[u_i \ v_i \ w_i]^T = [v_o \ 0 \ 0]^T$, so that:

$$v_{los,i} = l_{xi}u_i \quad (2)$$

Therefore, the longitudinal wind speed averaged over all the scan points yields:

$$u = \frac{1}{N} \sum_{i=1}^N \frac{v_{los,i}}{l_{xi}} \quad (3)$$

In the Spinner LiDAR case, $N=400$, and the beam directions change at every sample point following the rosette pattern, so $l_{xi} = \cos(\theta_i)$, where $\theta_i = [0 \ 30^\circ]$ is the cone half angle for the sample point. u is the Rotor Average Wind Speed (RAWS).

For control purposes, it is beneficial to remove the high frequency components of the measured wind so as to avoid unnecessary pitch actions. The filter is also necessary to remove any discontinuities introduced by the sampling pattern. In this project, the RAWS from (3) is filtered using a second order low-pass filter with a cut-off frequency of 3 rad/s and denominator damping ration of 1 to remove the discontinuities due to the sampling frequency.

The estimation of the longitudinal wind speed is affected by the fore-aft motion of the tower, so a correction factor must also be applied for the tower velocity. The output from the nacelle-mounted, or LiDAR's own accelerometer, is high pass filtered and integrated to provide a velocity. The velocity component along the beam direction is then subtracted to the measured line of sight velocity.

It should be noted that the estimate of the RAWS is performed at every controller cycle (100Hz), which means that in simulation, only 100 of the points in the rosette are actually used. This has a small effect on the RAWS estimate, as shown in the next section.

1.1.3. ESTIMATION RESULTS

The Rotor Average Wind Speed using the method above was tested against the true values provided by Bladed.

As mentioned above, only 100 out of 400 points per scan are used to estimate the RAWs. To see how well the RAWs are reconstructed, the estimation was first tested in steady wind conditions - with no turbulence, no wind shears, and no upflow – to ensure that it converges to the true value. Figure 2 shows the RAWs for a fictitious sinusoidal wind profile. As expected, in steady state, the estimation matches the true value.

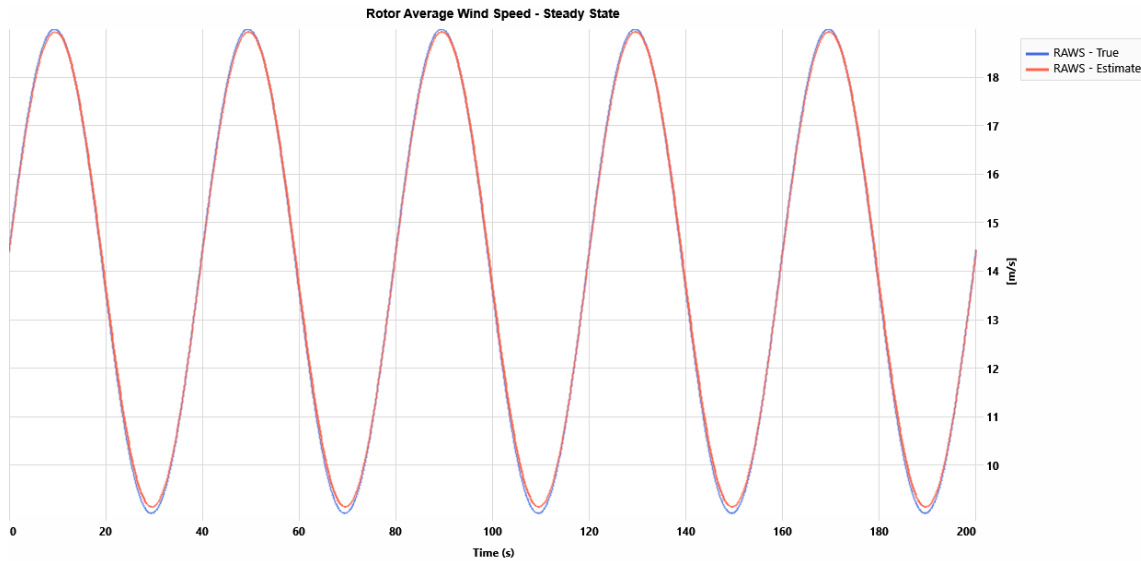
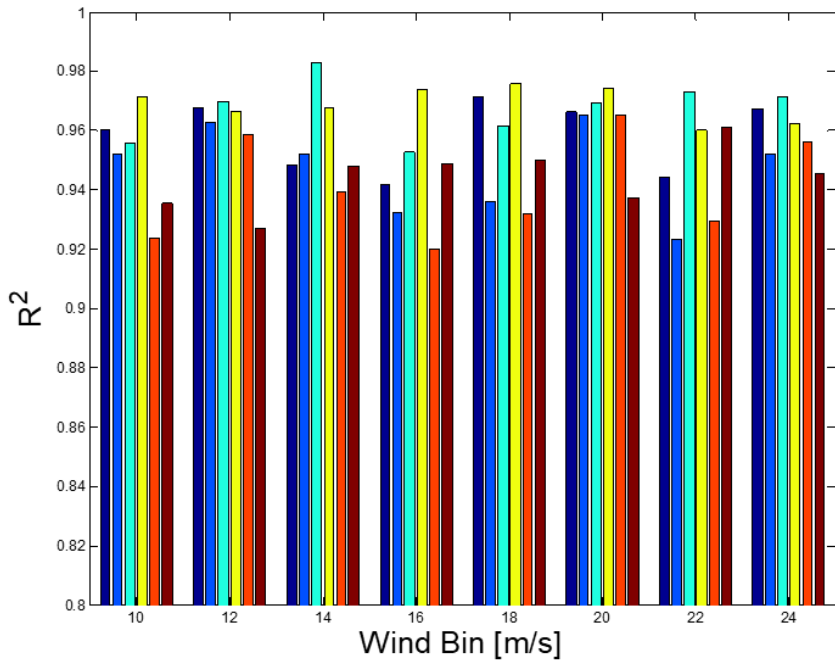
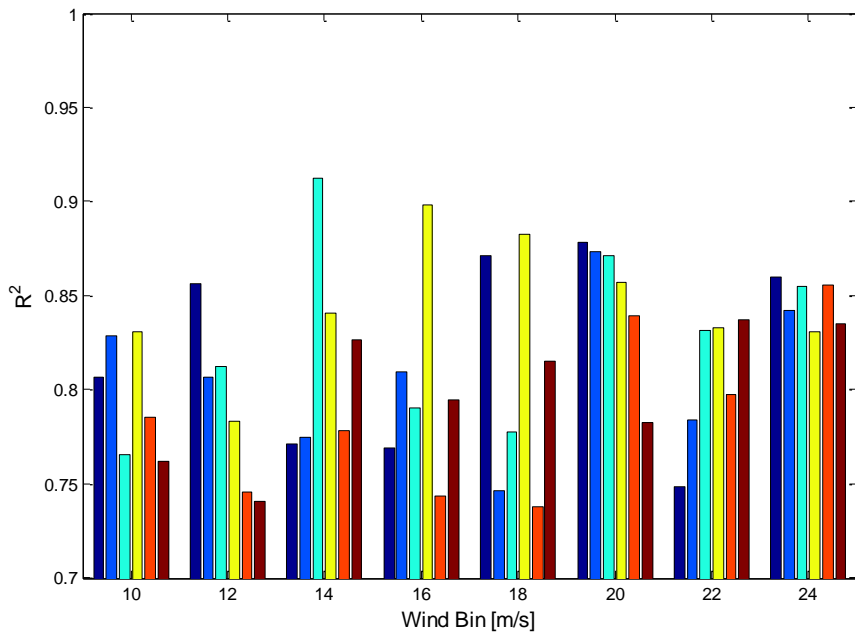


Figure 2 Rotor Average Wind Speed – steady state sine wave

In turbulent wind conditions, to assess wind reconstruction by the simulated LiDAR, the R-squared was computed for all the runs above rated in DLC 1.2 between estimates and true values of RAWs. Figure 3(a) shows the results for using the Taylor’s Frozen Turbulence assumption, while Figure 3(b) shows the results for the Evolving Turbulence [3]. In both cases the R-squared shows a reasonably good fit between estimates and true values, suggesting that even though only 100 points are used, there is no significant loss of fidelity.



(a) Frozen Turbulence



(b) Evolving Turbulence

Figure 3 DLC 1.2 – R² between true and estimated RAWS

Figure 4, shows the time series of estimated RAWS when using 400 points versus 100 points. This was obtained by increasing the controller cycle time in simulations to 400Hz and thus performing the estimation considering all of the points in the scan.

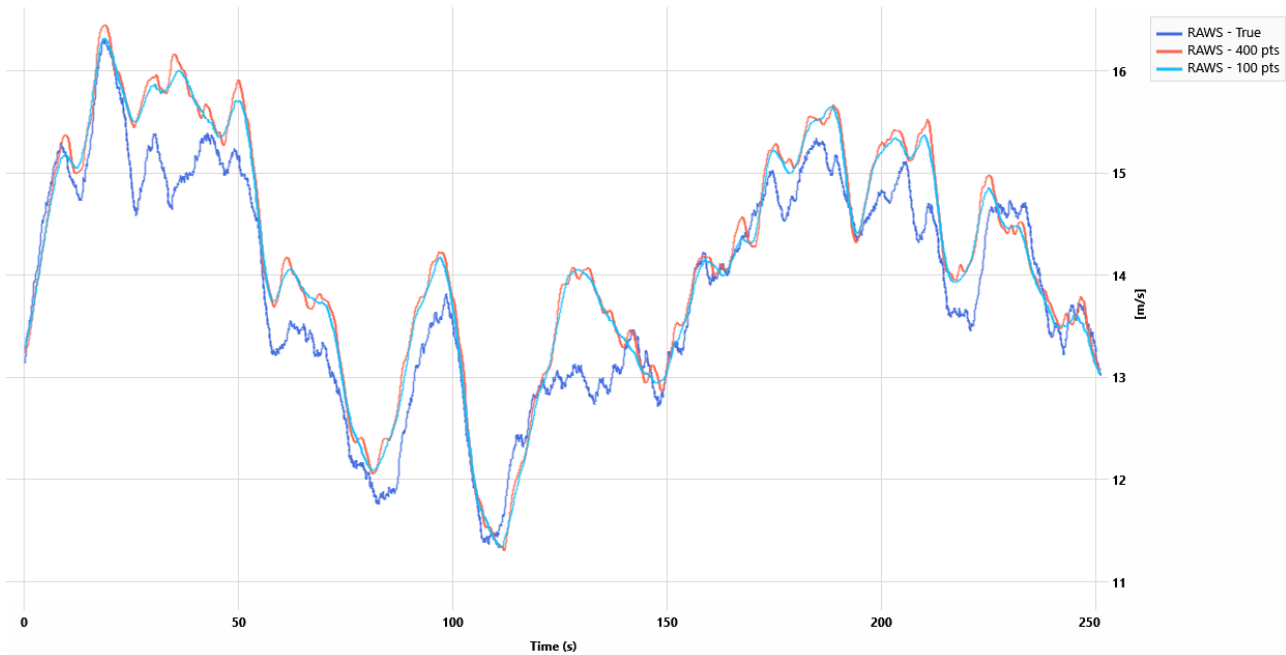


Figure 4 Difference in RAWS Estimate when using 100 points per scan versus 400 (Frozen Turbulence).

1.2. Feed Forward Algorithm

The feed-forward algorithm uses LIDAR preview measurement of longitudinal wind speed to determine a collective pitch control rate that allows the turbine to predictively react to variations in wind speed.

Collective pitch control is used principally to regulate the rotational speed to the rated value when operating above rated wind speed. However, any change to the blade pitch angle also has a major effect on out-of-plane rotor and fore-aft tower loads. Generally, relatively high-frequency pitch action is needed to minimise loads, while speed regulation can be achieved with lower-frequency action due to the large rotor inertia. The LIDAR preview information is well-suited to driving this low-frequency action, effectively freeing up the higher-frequency action to concentrate on load alleviation.

The controller implementation performs several actions before the pitch control rate is determined:

1. The RAWS, u , is estimated from the line-of-sight measurement at the focal points, as per Eq. (3).
2. A look-ahead time (T_{LA}) is determined, see (4) below.
3. The RAWS is then passed through a buffer and sorted according to the time expected before it reaches the rotor. The measurements are assumed to convect towards the turbine at the Convection Speed, V_c .
4. The RAWS in the buffer are interpolated to give a value corresponding to the look ahead time, and then are passed through a low pass filter to remove the high frequency components as explained in Section 1.1.2.
5. The feed forward pitch rate is determined and added to the closed loop control signal.

The subsequent sections will provide further details on point 2 and 5.

1.2.1. LOOK AHEAD TIME

The Look Ahead Time (LAT) is determined as:

$$T_{LA} = \frac{X_{dist}}{V_c} = \frac{f_d \cos(\theta_i)}{V_c} \quad (4)$$

Where:

- X_{dist} is the horizontal distance between the focal point and the rotor
- f_d is the beam focal length
- θ_i is the beam angle relative to the lidar axis
- V_c is the current Convection Speed, which is calculated passing u through a first order filter with a large time constant, $\tau = 20s$.

Eq. 4 gives the Maximum Look Ahead Time, but if required, a particular LAT, $T_{LA}^* < T_{LA}$, can be specified by the user. Since T_{LA} varies with the convection speed, the controller will use:

$$T_{LAC} = \min(T_{LA}^*, T_{LA}) \quad (5)$$

as the actual look ahead time.

For this project, a look ahead time of 5 seconds was used in the simulations.

1.2.2. FEED FORWARD PITCH RATE

The additional collective pitch rate is determined from the steady-state relationships between wind speed and pitch angle (see Figure 5) according to the following equation

$$\dot{\theta}_{FF}(t) = \frac{\hat{\theta}_{ideal}(t + \tau) - \theta(t)}{\tau} \quad (6)$$

Where:

- $\dot{\theta}_{FF}(t)$: feed forward pitch rate
- $\hat{\theta}_{ideal}(t + \tau)$: ideal pitch at LAT, given the LiDAR wind speed estimate
- $\theta(t)$: current pitch angle at the rotor
- $\tau = T_{LA}$: Look Ahead Time, as computed in (5). This can also be referred to as the Time-to-Rotor

It should be noted that the feed forward algorithm is only active in above rated conditions.

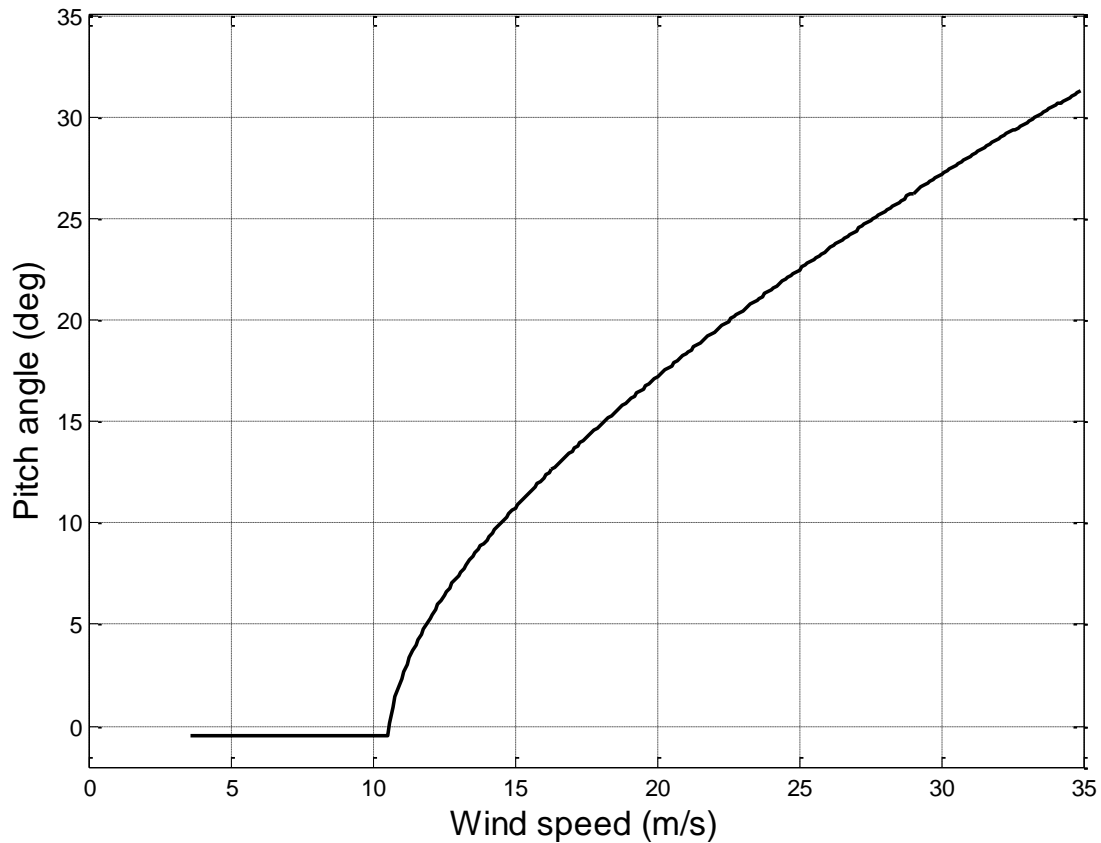


Figure 5 Steady state relationship between pitch angle versus wind speed

1.2.3. COLLECTIVE PITCH-SPEED CONTROLLER GAINS

Above rated wind speed, the pitch demand is varied in response to measured generator speed in order to maintain the speed set-point. This is achieved by means of a PI controller.

The PI controller takes the form

$$K_p(\beta) + \frac{K_i(\beta)}{s}, \tag{7}$$

where:

K_p = proportional gain;

K_i = integral gain;

The gains are calculated at each time-step from the current pitch angle β , through inverse interpolation (for K_p) or linear interpolation (for K_i) of the scheduled values that are stored in a look-up table.

The addition of the feed forward control allows detuning of these closed loop control gains to reduce turbine fatigue loading. Because the scope of the project is to retro-fit LiDAR Assisted

Control onto an existing turbine, the pitch speed controller gains were detuned in order to obtain a similar performance in terms of generator speed regulation.

1.3. Controller Performance

The PI gains of the LAC controllers were detuned trying to match the generator speed standard deviation (STD) and absolute max of the baseline controller. The tuning process was first performed with simulations using Frozen Turbulence assumptions, and then the controller was tested against the Evolving Turbulence – this was done due to the heavy computational load required by the latter caused by the large number of sampling points. Table 3 reports the performance comparison between the baseline and the LAC. In terms of standard deviation, the generator speed is very similar, with LAC providing slightly tighter speed regulation than the baseline. The gains could have been further relaxed to match exactly the baseline, but this would have incurred higher overspeeds. The maximum generator speed is higher than for the baseline case, but still within the existing alarm threshold of the turbine controller, which is 449 rpm.

During the field tests with LAC, the generator maximum should be monitored and the controller may need to be adjusted if frequent overspeeds are detected.

Figure 6 compares generator speed and pitch angle for a turbulent simulation at 16 m/s between “Baseline” and LAC controller. The mean pitch activity is significantly smoother for the LAC case (light blue) compared to the Baseline (yellow), which translates into lower Tower Base My (see Figure 7).

Table 3 Generator Speed Performance Comparison – Evolving Turbulence

		Wind Speed [m/s]	10	12	14	16	18	20	22	24
Gen Speed Std. Dev. [rpm]	Baseline		16.6	8.7	9.9	10.3	9.9	10.2	10.9	11.3
	LAC + De-tuned gains		18.1	10.2	10.3	9.3	8.7	9.2	11.0	12.1
Gen. Speed Absolute Max [rpm]	Baseline		421.2	427.8	434.0	440.8	436.4	445.4	443.5	443.8
	LAC + De-tuned gains		434.1	440.1	448.5	438.5	438.3	436.0	445.2	447.5

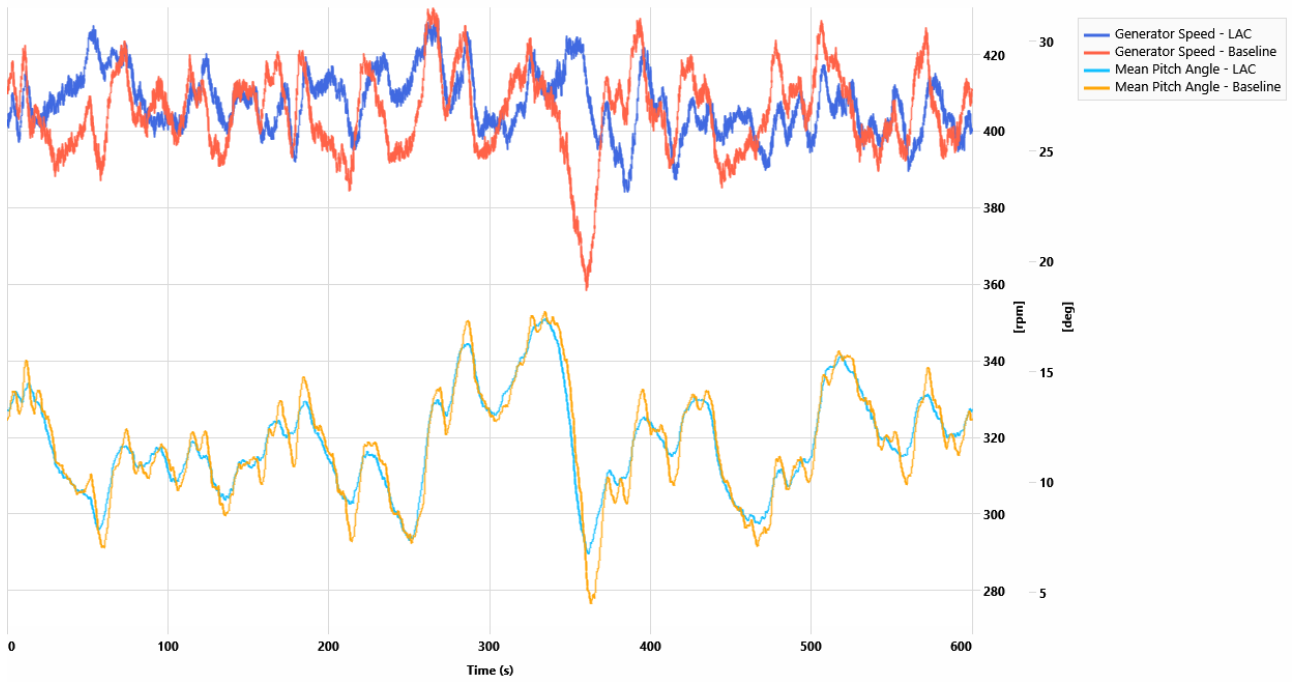


Figure 6 Controller Performance - Turbulent Simulation 16 m/s

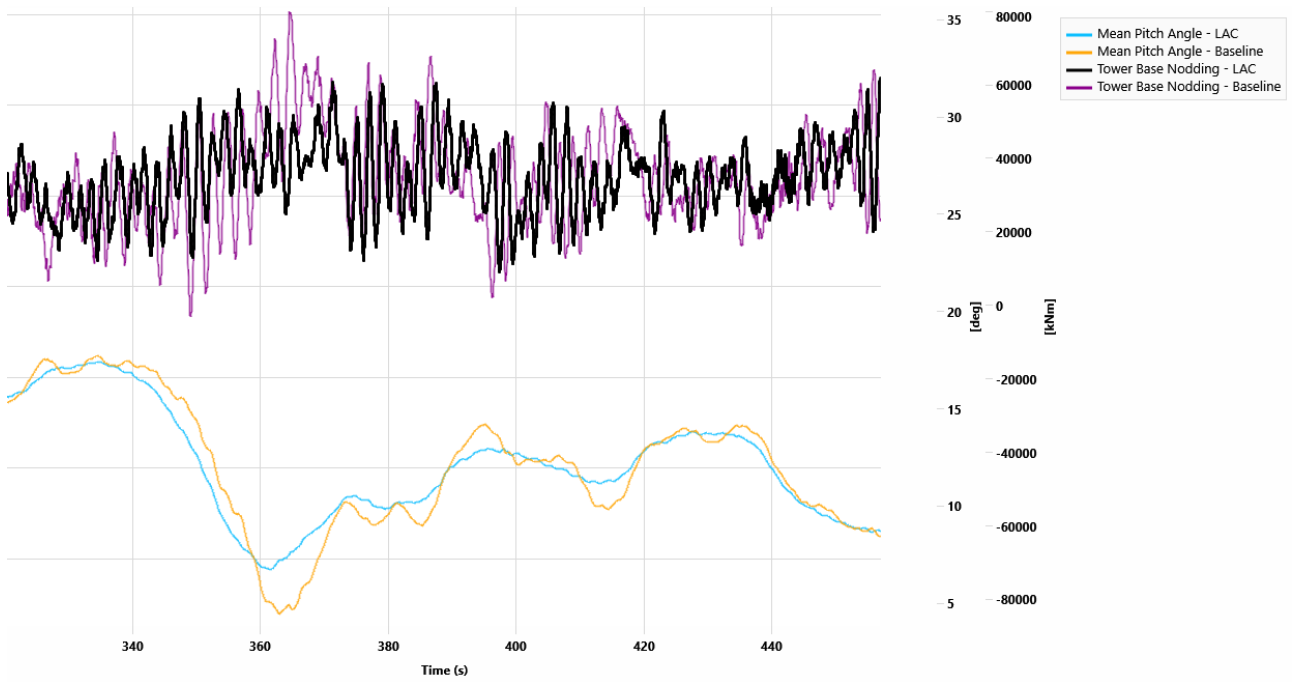


Figure 7 Controller Performance - Turbulent Simulation 16 m/s – Tower Base My

1.4. Fatigue Loads (DEL) Results

1.4.1. LOAD CASE DEFINITION

Power production calculations were set up according to the definition of design load case 1.2 in IEC61400-1 Edition 3, using the normal turbulence model. The wind class was IA. Table 4 describes DLC 1.2.

The partial safety factor for fatigue loads required by the IEC 61400-1 Ed. 3 standard is 1.0.

Table 4 Load Case Definition

Design load case (DLC): 1.2 Operating condition: Power production Wind conditions: Normal turbulence model, $3 < V_{hub} < 25\text{m/s}$ Type of analysis: Fatigue Description of simulations:				
	Mean wind speed (m/s) (mid bin)	Longitudinal turbulence intensity (%)	Wind bin size (m/s)	Wind direction (deg)
aaa1-2	4	34.44	3 - 5	-8
aab3-4				0
aac5-6				8
aba1-2	6	26.93	5 - 7	-8
abb3-4				0
abc5-6				8
aca1-2	8	23.20	7 - 9	-8
acb3-4				0
acc5-6				8
ada1-2	10	20.96	9 - 11	-8
adb3-4				0
adc5-6				8
aea1-2	12	19.47	11 - 13	-8
aeb3-4				0
aec5-6				8
afa1-2	14	18.50	13 - 15	-8
afb3-4				0
afc5-6				8
aga1-2	16	17.60	15 - 17	-8
agb3-4				0
agc5-6				8
aha1-2	18	16.98	17 - 19	-8
ahb3-4				0
ahc5-6				8
aia1-2	20	16.48	19 - 21	-8
aib3-4				0
aic5-6				8
aja1-2	22	16.07	21 - 23	-8
1.2jb3-4				0
1.2jc5-6				8
1.2ka1-2	24	15.73	23 - 25	-8
1.2kb3-4				0
1.2kc5-6				8

1.4.2. DAMAGE EQUIVALENT LOADS

Damage equivalent loads are used to equate the fatigue damage represented by rainflow cycle count data to that caused by a single stress range repeating a fixed number of times. The method is based on the Miner’s rule. The damage equivalent stress is given by the following formula:

$$L_N = \sqrt[m]{\frac{\sum L_i^m n_i}{N}}$$

where L_N is the equivalent stress for N cycles

L_i is the stress range bin i.

n_i is the number of rain flow cycles at stress range bin i.

m is the negative inverse of the slope on the material’s Wöhler curve (m is also referred to as the S-N curve slope).

N is the number of cycle repetitions in the turbine lifetime.

The S-N curve slopes (m) used here are integer values from 3 to 12, where 4 typically represents steel and 10 typically represents glass reinforced plastic (GRP).

The stress, L_i , depends upon the geometry of the structure under consideration. It is assumed that stress is proportional to load, therefore it is quite acceptable to use load instead of stress in the above equation.

For simplicity, L_i and n_i have been derived from the one-dimensional table with no correction to account for the fatigue damage due to mean stresses.

The lifetime-integrated damage equivalent fatigue loads have been calculated for a reference frequency of 0.015844Hz corresponding to 1.0×10^7 cycles in 20 years. All damage equivalent moments and forces are presented in kNm and KN respectively.

The loads below were obtained running simulations in Bladed 4.8 and with Evolving Turbulence.

Figure 8 shows the average reduction in tower base bending moment in the fore-aft direction. The LAC controller reduces the loads systematically across all wind speeds in which the pitch controller is active, and it shows a reduction between 7-9% for wind speeds around and above rated. Near cut out (24 m/s) a Look Ahead Time of 5 seconds is not suitable, and simulations were showing overspeeds higher than the alarm threshold, so it was decided to phase out the feedforward algorithm in high wind speeds, and thus the reductions in DEL are less marked there than for the other wind bins.

Table 5 to Table 7 report the the Lifetime Equivalent Load for different components of interest. Overall, both tower base and blade root show a good reduction in fatigue loading, while tower top loading is largely unchanged.

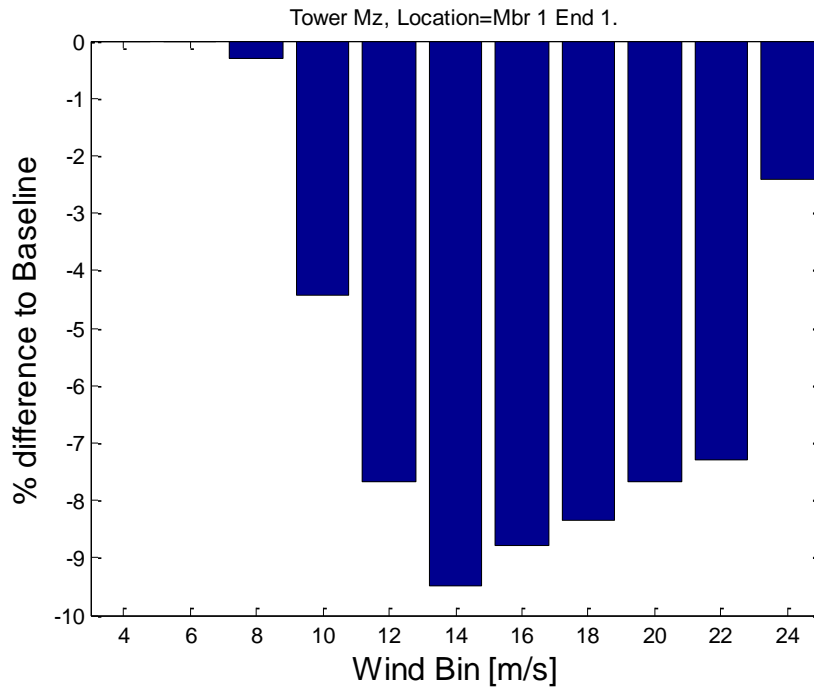


Figure 8 Damage Equivalent Load - average Reduction in Tower Base fore-aft moment (m=4)

Table 5 Lifetime weighted equivalent loads - Tower base – Percent Difference to Baseline

m	Mx [kNm]	My [kNm]	Mz [kNm]	Fx [kN]	Fy [kN]	Fz [kN]
3	0.3%	-4.0%	-5.1%	1.0%	-2.0%	-3.0%
4	0.2%	-4.8%	-5.7%	0.7%	-2.9%	-3.8%
10	-0.7%	-13.6%	-4.6%	0.1%	-4.4%	-11.8%

Table 6 Lifetime weighted equivalent loads – Tower Top – Percent Difference to Baseline

m	Mx [kNm]	My [kNm]	Mz [kNm]	Fx [kN]	Fy [kN]	Fz [kN]
3	0.3%	-0.7%	0.2%	1.0%	-4.6%	-3.6%
4	0.2%	-0.9%	-0.1%	0.7%	-5.6%	-4.4%
10	-0.6%	-1.9%	-1.5%	0.1%	-5.4%	-12.0%

Table 7 Lifetime weighted equivalent loads – Blade Root – Percent Difference to Baseline

m	Mx [kNm]	My [kNm]	Mz [kNm]	Fx [kN]	Fy [kN]	Fz [kN]
3	0.1%	-2.1%	-0.1%	-1.0%	0.2%	0.1%
4	0.1%	-2.9%	-0.3%	-1.7%	0.1%	0.0%
10	0.0%	-3.7%	0.5%	-2.8%	0.1%	0.3%

2. TOWER TOP IPC

Individual-pitch control (IPC) for wind turbines is a mature control feature applied to achieve reductions in asymmetric fatigue loading of turbine rotor/nacelle assemblies (RNA). Typical commercial implementations of IPC use blade-root based load sensing to provide feedback for IPC algorithms; however, the cost of the sensors themselves together with the cost of installation/maintenance and the additional pitch activity limited widespread usage of IPC in the industry [4] historically.

In this work, an alternative approach to IPC, which uses strain gauges mounted on the tower, was implemented in the Samsung 7MW turbine controller. Strain gauges mounted on the tower have the advantage being much more easily accessible, and they measure directly tower nodding and yawing moments, which IPC tries to minimise.

2.1. Theory

The conventional method for IPC uses blade root mounted sensors to measure out-of-plane bending moments (OOP), which are used to compute the individual pitch demands to reduce asymmetric loads of the rotor. The blade-root loads can be transformed into a non-rotating frame of reference using the Coleman transformation [5], which is also referred to as the d-q plane, to create three decoupled rotor loading signals: collective, cosine-cyclic, sine-cyclic:

$$\begin{bmatrix} M_{col,i} \\ M_{cos,i} \\ M_{sin,i} \end{bmatrix} = \begin{bmatrix} \frac{1}{3} & \frac{1}{3} & \frac{1}{3} \\ \frac{2}{3} \cos(i\psi) & \frac{2}{3} \cos\left(i\left(\psi + \frac{2\pi}{3}\right)\right) & \frac{2}{3} \cos\left(i\left(\psi + \frac{4\pi}{3}\right)\right) \\ \frac{2}{3} \sin(i\psi) & \frac{2}{3} \sin\left(i\left(\psi + \frac{2\pi}{3}\right)\right) & \frac{2}{3} \sin\left(i\left(\psi + \frac{4\pi}{3}\right)\right) \end{bmatrix} \begin{bmatrix} M_{y1} \\ M_{y2} \\ M_{y3} \end{bmatrix} = T(\psi, i) \begin{bmatrix} M_{y1} \\ M_{y2} \\ M_{y3} \end{bmatrix} \quad (8)$$

Where i is the transformation order, $M_{col,i}$ is the i^{th} order collective rotor load; $M_{cos,i}$ is the i^{th} order cosine-cyclic rotor load; $M_{sin,i}$ is the i^{th} order sine-cyclic rotor load; ψ is the rotor azimuth and, M_y is the OOP moment measured by the strain gauges on each blade.

In the case of a first order transformation, the resulting loads are closely correlated to Hub Thrust (Hub Fx), tilting moment (Hub My) and yawing moment (Hub Mz).

These asymmetric loading signals can then be used in feedback through separate IPC controllers to create cyclic pitch demands, by transforming back into the rotating frame through an inverse transformation:

$$\begin{bmatrix} \Delta\theta_1 \\ \Delta\theta_2 \\ \Delta\theta_3 \end{bmatrix} = \sum_{i=1}^n T(\psi, i)^{-1} \begin{bmatrix} K_{cos,i}(M_{cos,i}) & 0 \\ 0 & K_{sin,i}(M_{sin,i}) \end{bmatrix} \quad (9)$$

Where $\Delta\theta_i$ is the pitch demand for blade i , $K_{cos,i}$ and $K_{sin,i}$ are the controller for the cosine-cyclic and sine-cyclic loads after an i^{th} order transformation. For this work, the controllers are implemented as Proportional-Integral (PI controllers).

In practice, because of time delays and actuator response, the pitch perturbation does not reach the maximum value exactly at the azimuth angle at which it was computed. Also, because of the

structural and aerodynamic responses, the effect on the load is felt at some later azimuth angle. To account for this phase shift between the pitch demand and the desired effect on the load, a corresponding phase shift is introduced to the pitch angles calculated from equation (9).

The order of the transformation defines the rotor harmonic at which the pitch angle demands will modulate the loads. Table 8 indicates the loading frequencies targeted by IPC in the rotating (e.g. Blades) and non-rotating (e.g. Stationary Hub) up to the second order transformation

Table 8 Targeted load frequencies

	Rotating	Non-rotating
1st Order	1P	0P
2nd Order	1P+2P	0P+3P

2.2. Tower Top IPC

As mentioned earlier, when using blade root sensors, a transformation into the non-rotating frame resolves the individual blade root loads into out-of-plane rotor collective, tilt, and yaw loading, which are then used to compute the pitch demands that reduce them.

A more direct and possibly cost-effective approach would be to measure the loads directly into the non-rotating frame. Using strain gauges mounted on the tower top can yield the required measurements. However, it should be noted that IPC targets tilt and yaw moments in the stationary hub coordinate system. If the sensors are moved away from the origin of this reference frame, then additional moments will be applied to the sensors, as shown in Figure 9. These moments will need to be subtracted from the measured signals, otherwise the controller will try reduce their effect and therefore unbalance the rotor [4].

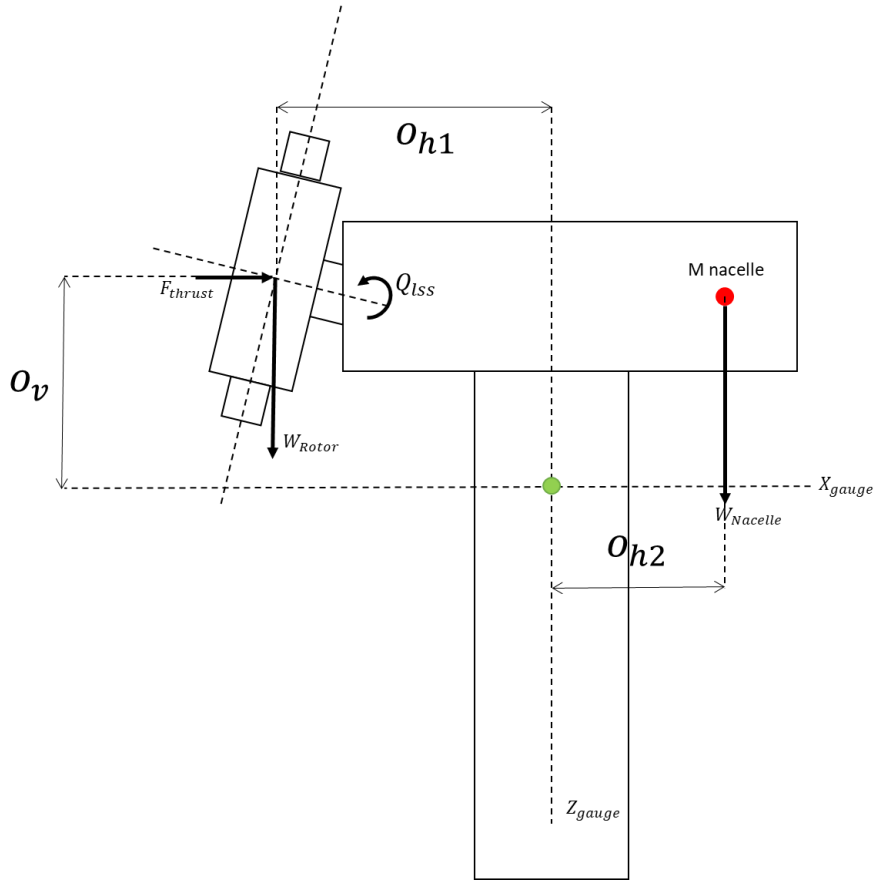


Figure 9 Side schematic of Hub/Nacelle/Tower Assembly

The hub tilt and yaw loads (which approximate closely with $M_{cos,i}$ and $M_{sin,i}$ respectively) can be estimated from the tower top load measurements according to:

$$M_y = Q_y - (F_{thrust}o_v + W_{Nacelle}o_{h2} - W_{rotor}o_{h1}) \quad (10)$$

$$M_z = Q_z - Q_{lss} \sin(\theta_{tilt}) \quad (11)$$

Where M_y and M_z are the estimate of stationary Hub tilt and yaw moment, respectively, Q_y is the measured tower tilt moment, F_{thrust} is the rotor collective thrust load, Q_z is the measured tower yaw moment, Q_{lss} is the low-speed shaft torque and θ_{tilt} is the low speed shaft tilt angle.

At low frequencies, Q_{lss} can be approximated by the demanded generator torque through the gearbox:

$$Q_{lss} \approx Q_{gen}N \quad (12)$$

The thrust force can be approximated solving the quasi-steady-state thrust equation:

$$F_{thrust} = \frac{1}{2} \rho A C_t(V, \omega_r, \theta_{col}) V^2 \quad (13)$$

Where ρ is the air density, A is the rotor area, C_t is the coefficient of thrust, ω_r is the rotor speed and V is the effective wind speed. A Luenberger wind-speed estimator based on that presented in [6] was used to estimate wind speed, and C_t solved using a look-up table derived from a *Bladed*

steady state calculation. The geometrical and physical parameters of the Samsung 7MW turbine are reported in Table 9.

Table 9 Physical parameters of the Samsung 7MW turbine

Overhang, o_{h1}	7.78 m
Nacelle C.M. Offset, o_{h2}	0 m
Rotor-Gauges Vertival Offset, o_v	5.1 m
Rotor Diameter, d	171.14 m
Gearbox ration, N	38.3
Rotor and HubMass, M_{rotor}	209,930 kg
Nacelle Mass	342,000 kg
Tilt Angle, θ_{tilt}	5 deg
Tower Height, h	80 m
Strain Gauges Height, h_{gauges}	78.5 m

As can be seen in Figure 10 and Figure 11, with the method above the strain gauges provide a good estimate of the Stationary Hub tilt and yaw moments, which can then be used to compute the 1P Tower Top (TT) IPC pitch perturbations as described in Section 2.1.

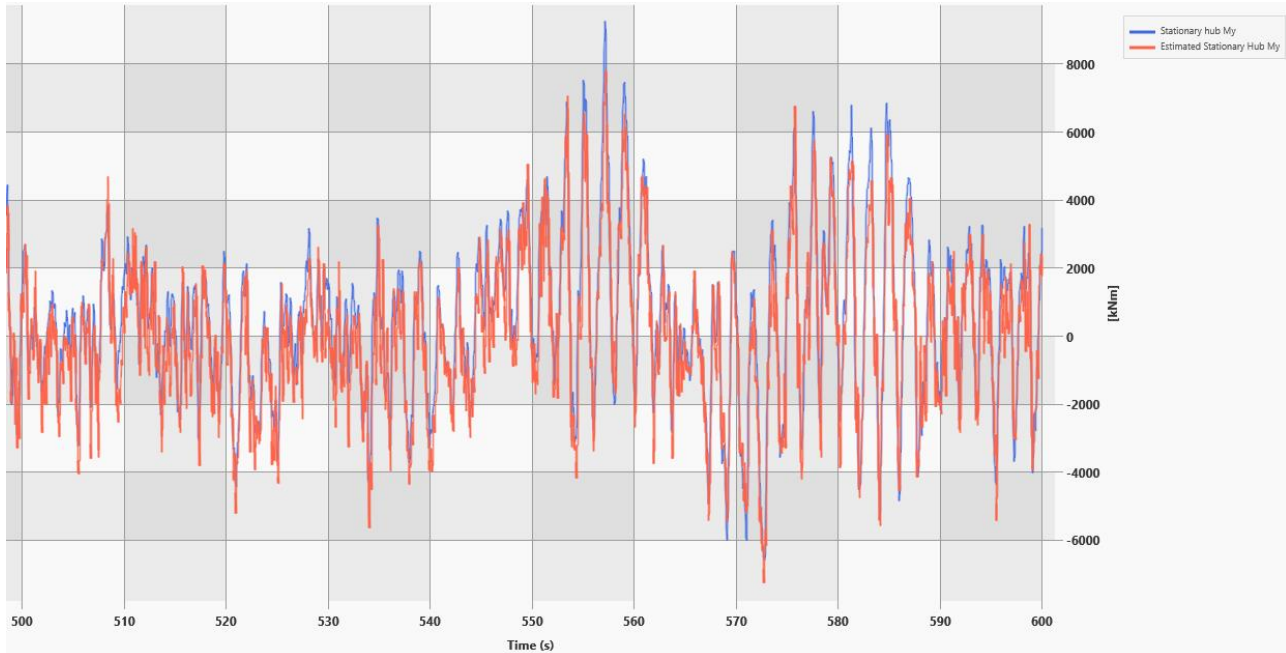


Figure 10 Estimated (orange) and Actual Stationary (blue) Hub My

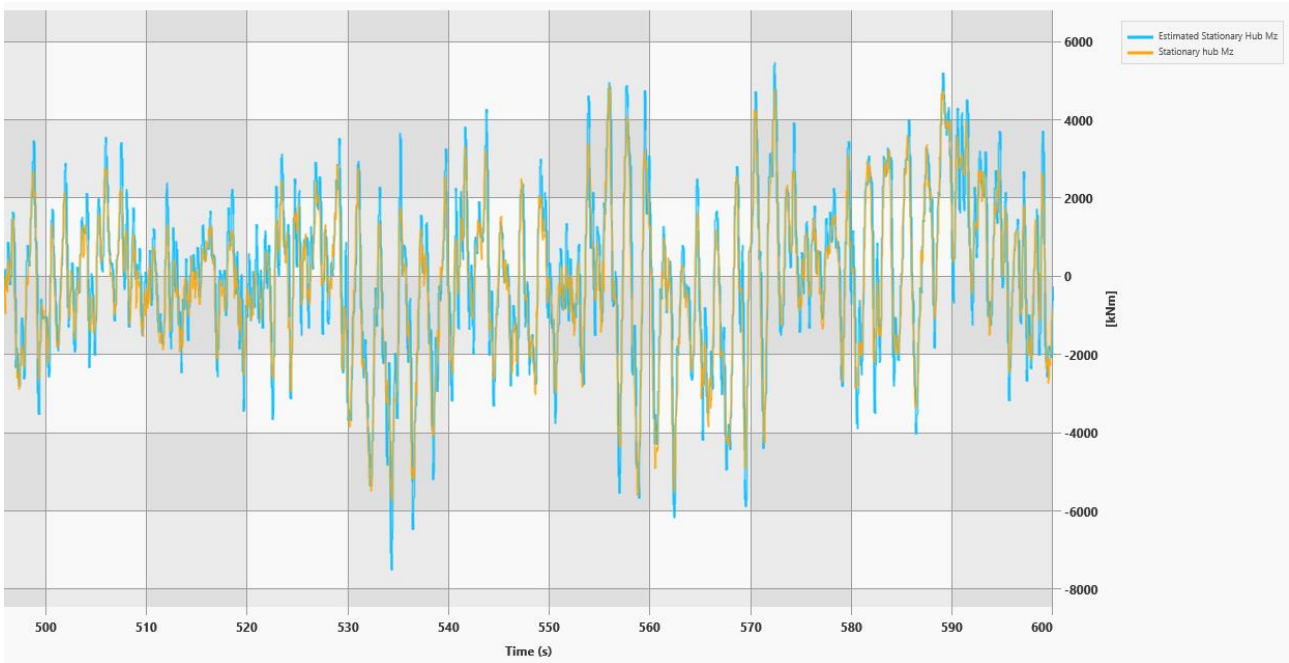


Figure 11 Estimated (ligh blue) and Actual Stationary (yellow) Hub Mz

2.2.1. SPECTRAL ANALYSIS

The PI gains of the 1P TT IPC control loop were tuned to have a similar performance as the conventional IPC with blade root sensors (1P BR IPC), and the same IPC amplitude was used in simulations.

Figure 12 and Figure 13 compares the autospectra of Stationary Hub tilting (My) and yawing (Mz) moment for the two IPC strategies. As can be seen, they both reduce the spectra content at 0P by one order of magnitude compared to no IPC, with the TT IPC closely matching BR IPC.

Figure 14 shows the autospectra of blade 1 root My. Both IPC strategies show a significant reduction of the 1P load (0.19Hz). The TT IPC controller does show a small peak at 1P relative to BR IPC which may be due to targeting the the hub load balancing rather than the blade load balancing.

The blade 1 pitch angle spectra (Figure 15) shows a large increase at 1P, as expected, with the TT IPC showing a smaller peak compared to BR IPC.

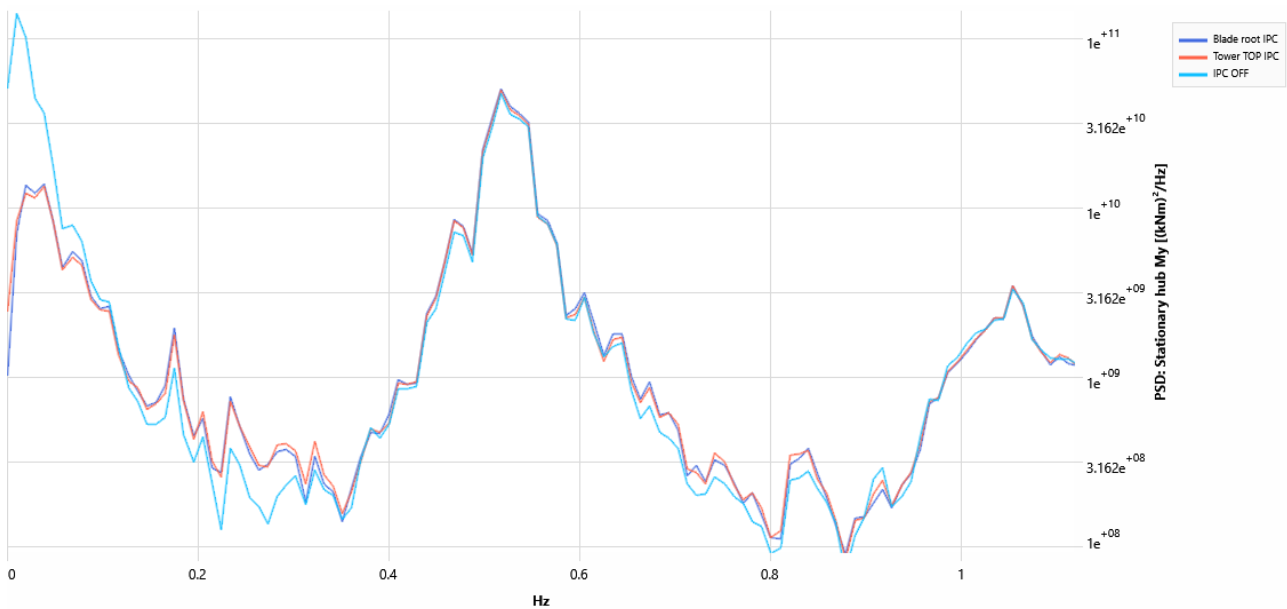


Figure 12 Effect on Stationary Hub My of 1P IPC. Blade root sensors (blue) and tower top sensors (orange)

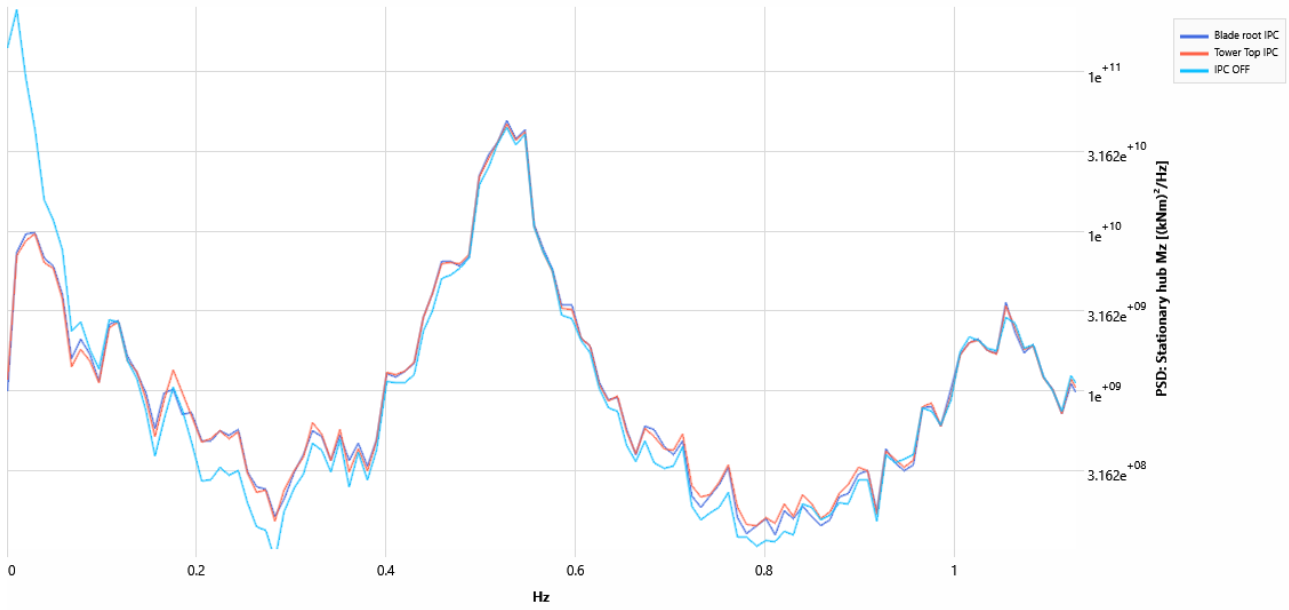


Figure 13 Effect on Stationary Hub Mz of 1P IPC. Blade root sensors (blue) and tower top sensors (orange)

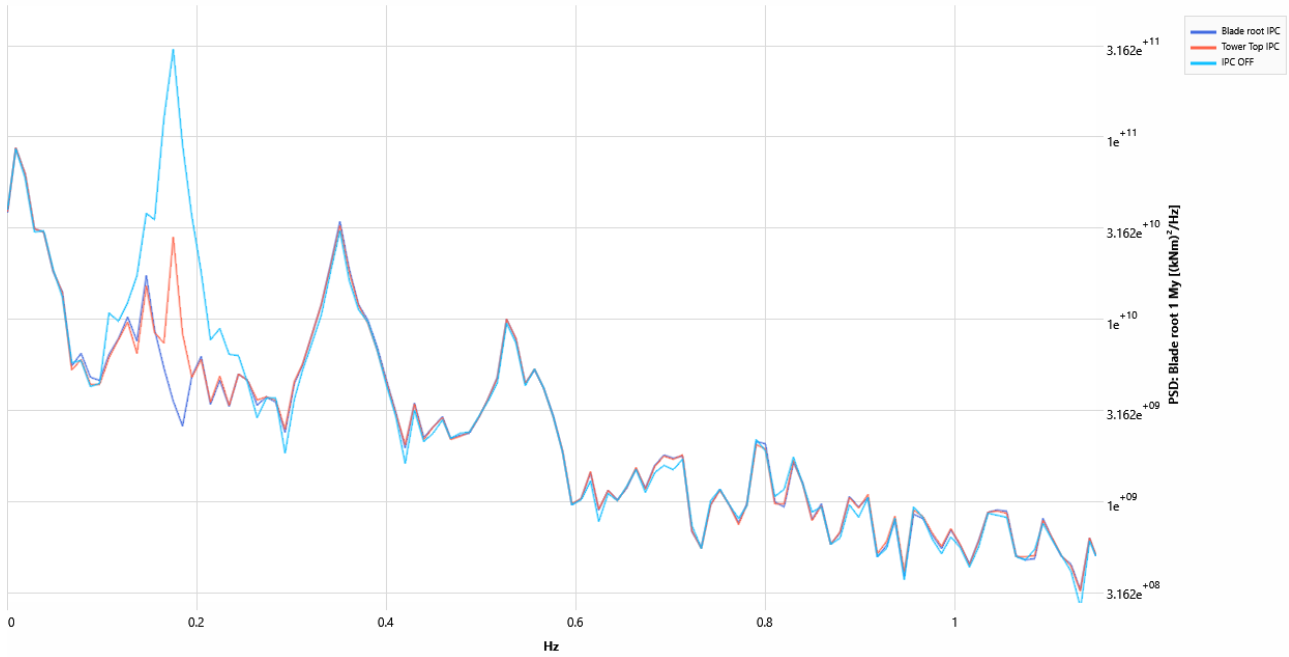


Figure 14 Effect on Blade Root My of 1P IPC. Blade root sensors (blue) and tower top sensors (orange)

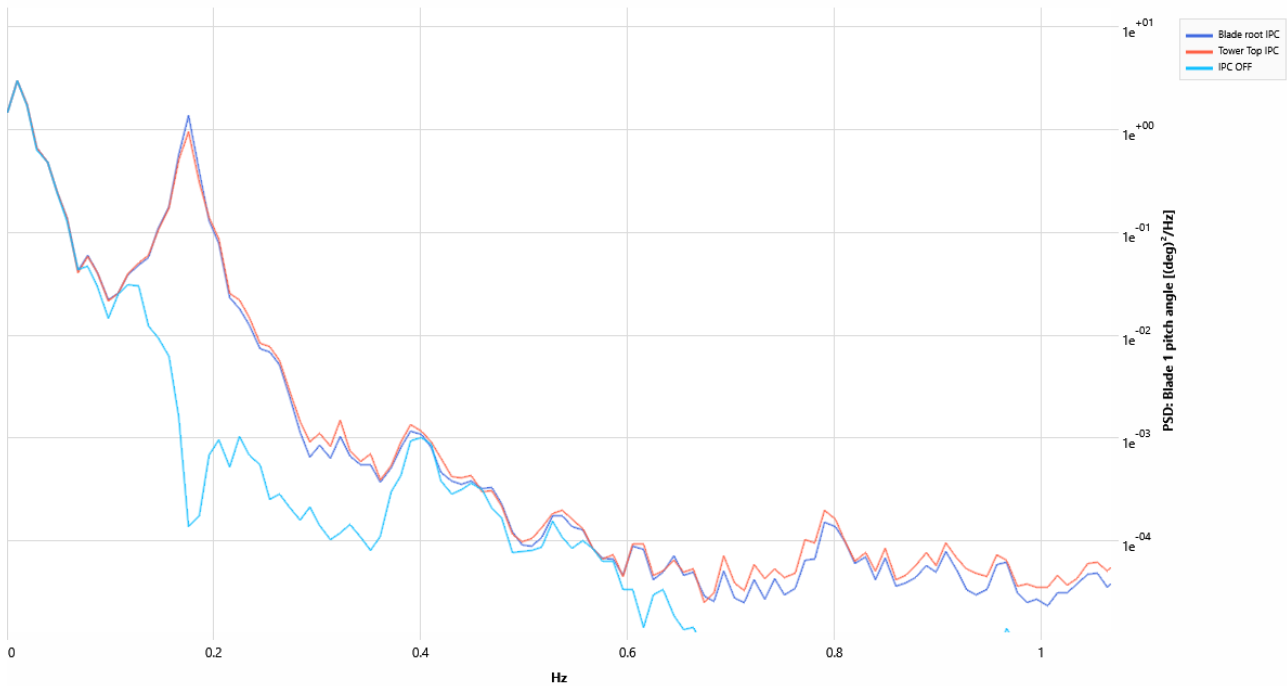


Figure 15 Effect on Blade 1 pitch angle of 1P IPC. Blade root sensors (blue) and tower top sensors (orange)

2.2.2. FATIGUE LOADS (DEL) RESULTS

Relative to no IPC, the damage equivalent loads for major components considered at each wind speed are shown in Figure 16 to Figure 21. The blade root loads for both $m=4$ and $m=10$ show significant reductions with respect to the no IPC case, with the TT IPC showing slightly less load reductions for both $m=4$ and $m=10$ compared to BR IPC.

The stationary hub M_y and M_z loads are higher for the BR IPC case, which is consistent with the expectations since TT IPC targets the loads in the stationary frame by measuring directly the required signals. In the yaw bearing, a similar trend can be seen.

Overall the the IPC strategies show very similar levels of load reductions, sugeting no theoretical disadvantages in employing tower top sensors for 1P IPC.

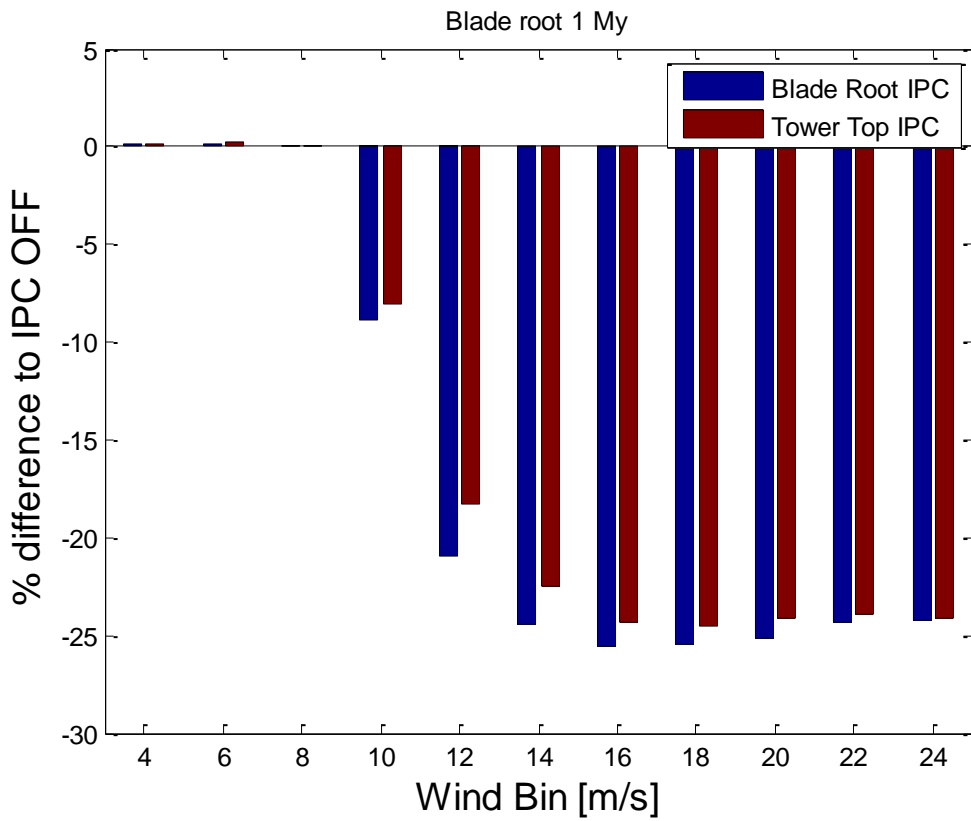


Figure 16 Relative change in blade 1 root My DEL (m=4)

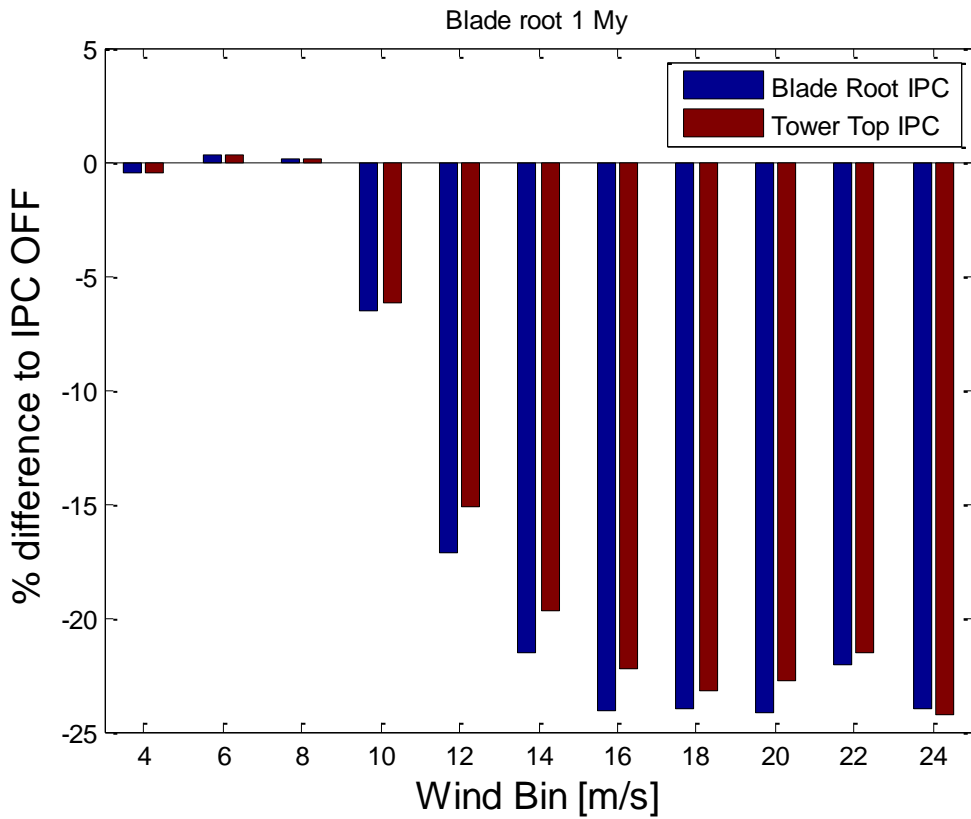


Figure 17 Relative change in blade 1 root My DEL (m=10)

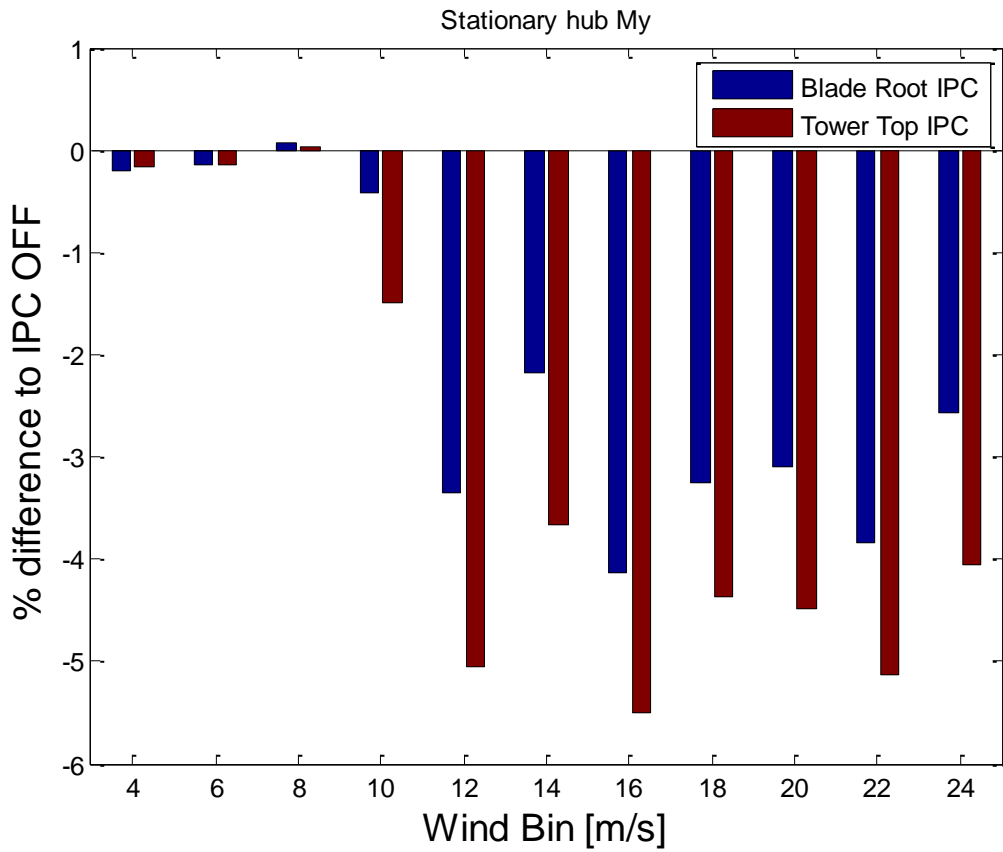


Figure 18 Relative change in Stationary Hub My DEL (m=4)

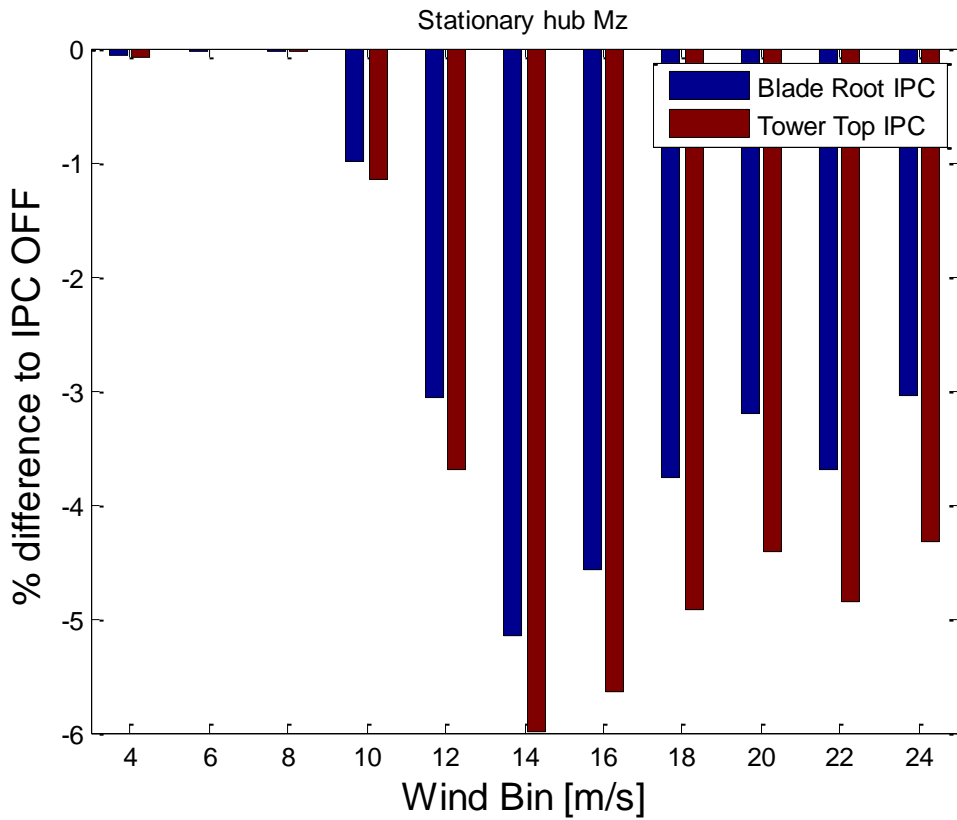


Figure 19 Relative change in Stationary Hub Mz DEL (m=4)

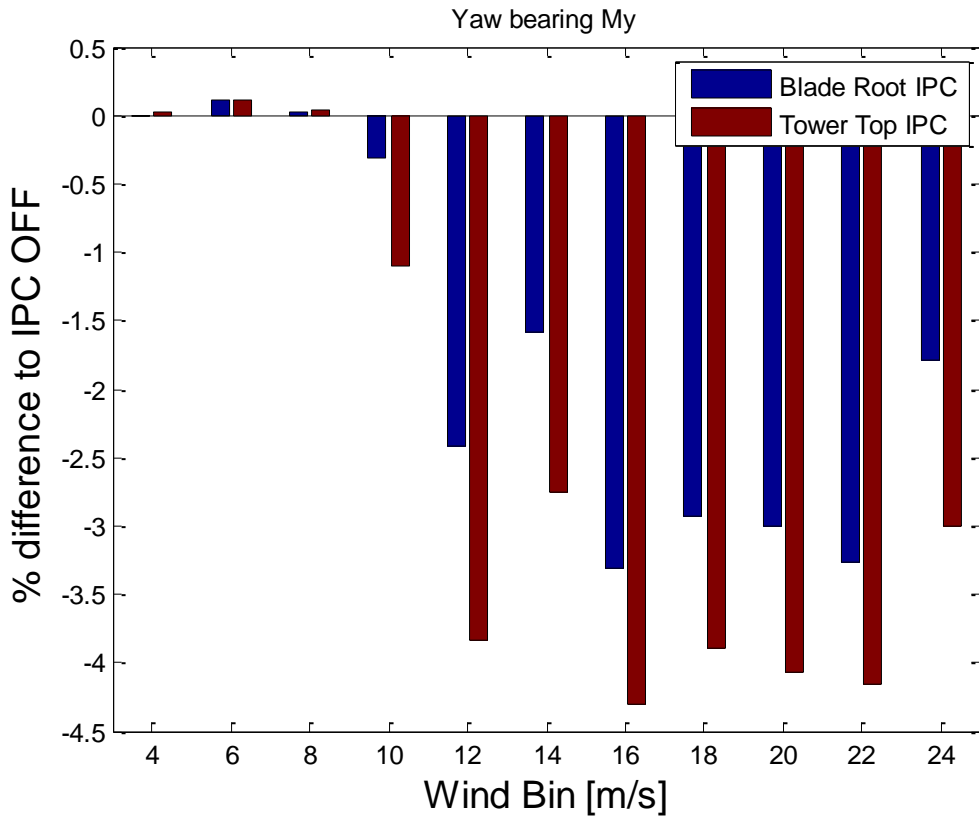


Figure 20 Relative change in Yaw Bearing My DEL (m=4)

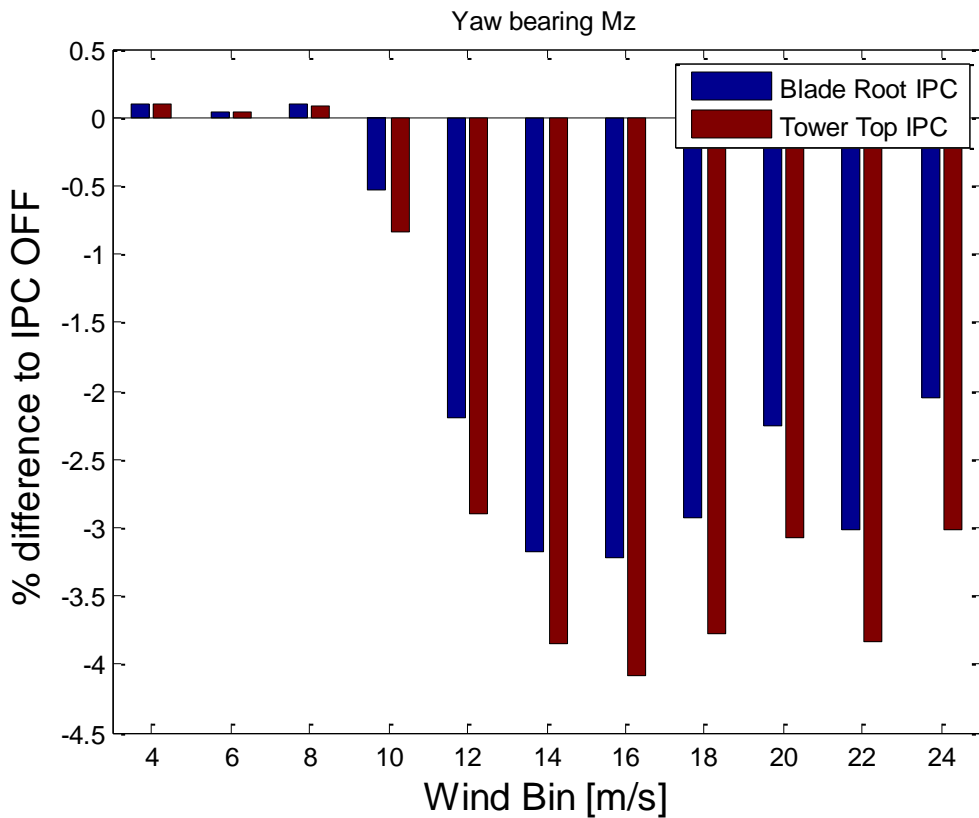


Figure 21 Relative change in Yaw Bearing Mz DEL (m=4)

2.3. 2P IPC

The Samsung 7MW turbine was not designed to include 2P IPC, so for the purposes of this study, a second order IPC controller loop was designed and added to turbine controller.

First, the 2P IPC was designed using the blade root sensors. A sensitivity study was done to establish the pitch amplitude that best reduced the loads while keeping the added pitch activity as low as possible. Figure 22 shows the autospectrum of Stationary Hub My, and Figure 23 shows the cumulative variance in blade 1 pitch rate for 0.5, 1 and 2 deg amplitudes. Clearly, all three amplitudes reduce the spectra at 3P(0.57Hz), but there is no further benefit in increasing the amplitude further than 1 deg, so this was selected as the 2P IPC maximum perturbation.

In the case of tower top 2P IPC, a reverse transformation is first applied to go from the non-rotating frame to the rotating frame (effectively converting the Tower top measurements in estimates of blade root loading). Then, a second order transformation is applied to translate the loads into a 2P d-q axis:

$$\begin{bmatrix} 0 \\ M_{cos,i} \\ M_{sin,i} \end{bmatrix} = T(\psi, 2)T(\psi, 1)^{-1} \begin{bmatrix} 0 \\ M_y \\ M_z \end{bmatrix} \tag{14}$$

In this process, the collective component is assumed to be zero since it's not used for IPC in any case.

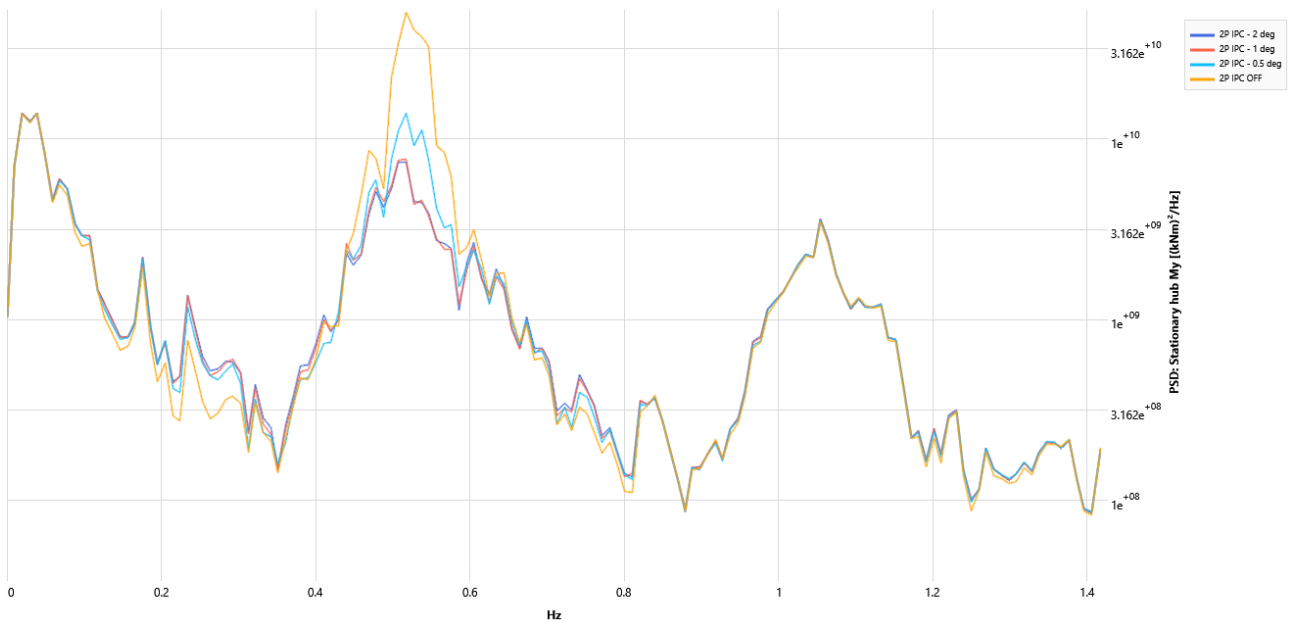


Figure 22 Reduction in Stationary Hub My at 3P with different 2P IPC amplitudes. 0.5 deg (light blue), 1 deg (orange), 2 deg (blue)

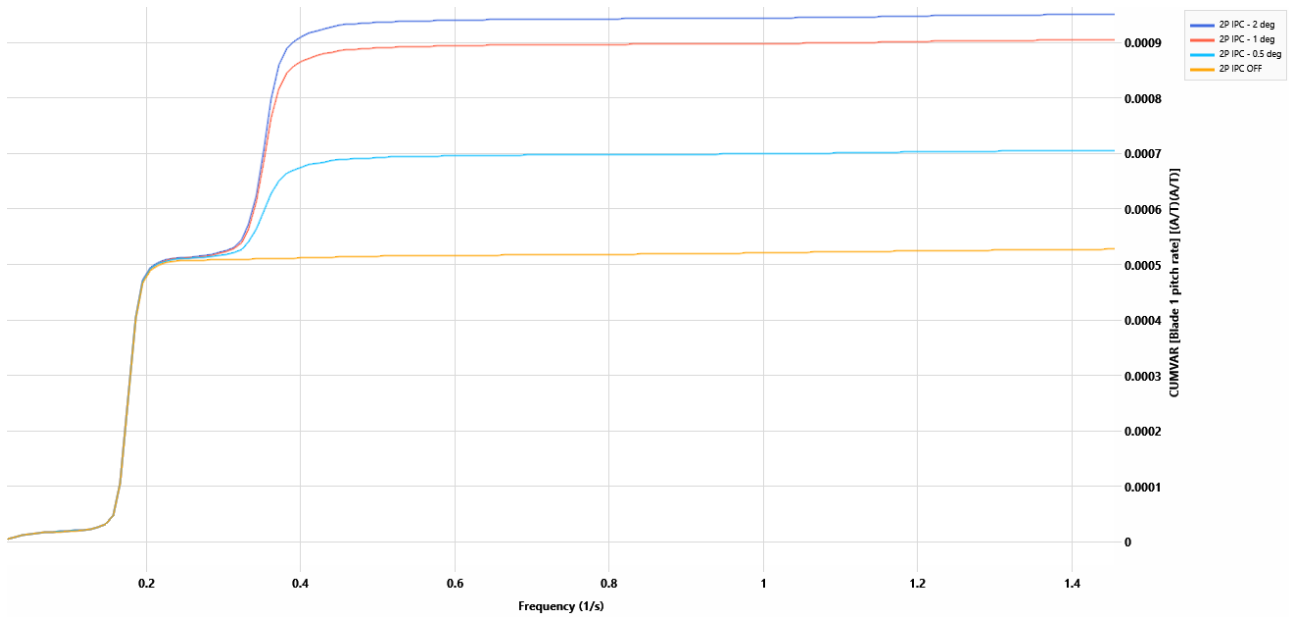


Figure 23 Cumulative variance of pitch rate with different 2P IPC amplitudes. 5 deg (light blue), 1 deg (orange), 2 deg (blue)

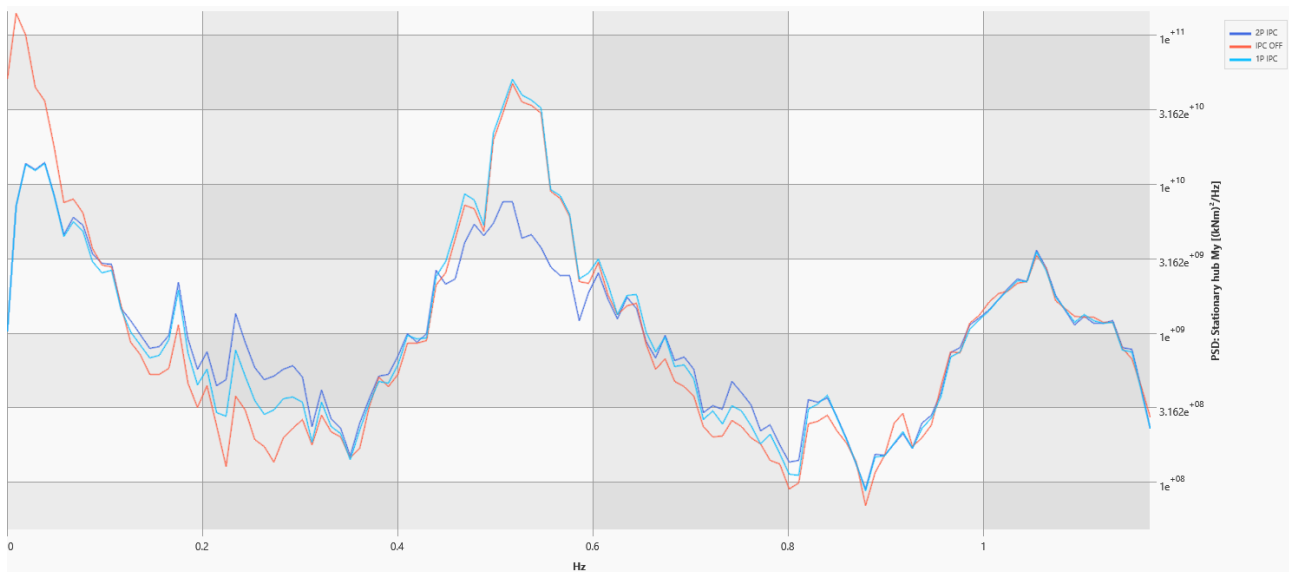


Figure 24 Effect on Stationary Hub My of 2P IPC with Blade root sensors.

2.3.1. SPECTRAL ANALYSIS

The 2P IPC control loops for blade root and tower top were tuned to have similar performance. Figure 25 and Figure 26 compare the autospectra of Stationary Hub tilting (My) and yawing (Mz) moment for the two IPC strategies. As can be seen, they both reduce the spectral content at 3P compared to no IPC, with the BR IPC showing a better reduction than TT IPC. The transformation

from stationary frame to rotating and back to stationary can introduce an array of sources of uncertainty, considering as well that the Tower Top measurements are themselves estimates of the actual values, so a drop in performance is somewhat expected, and it becomes clear in Section 2.3.2.

Blare root My also shows higher activity at 2P for TT IPC compared to BR IPC (Figure 27), while pitch rate shows similar levels of increase for both strategies (Figure 28).

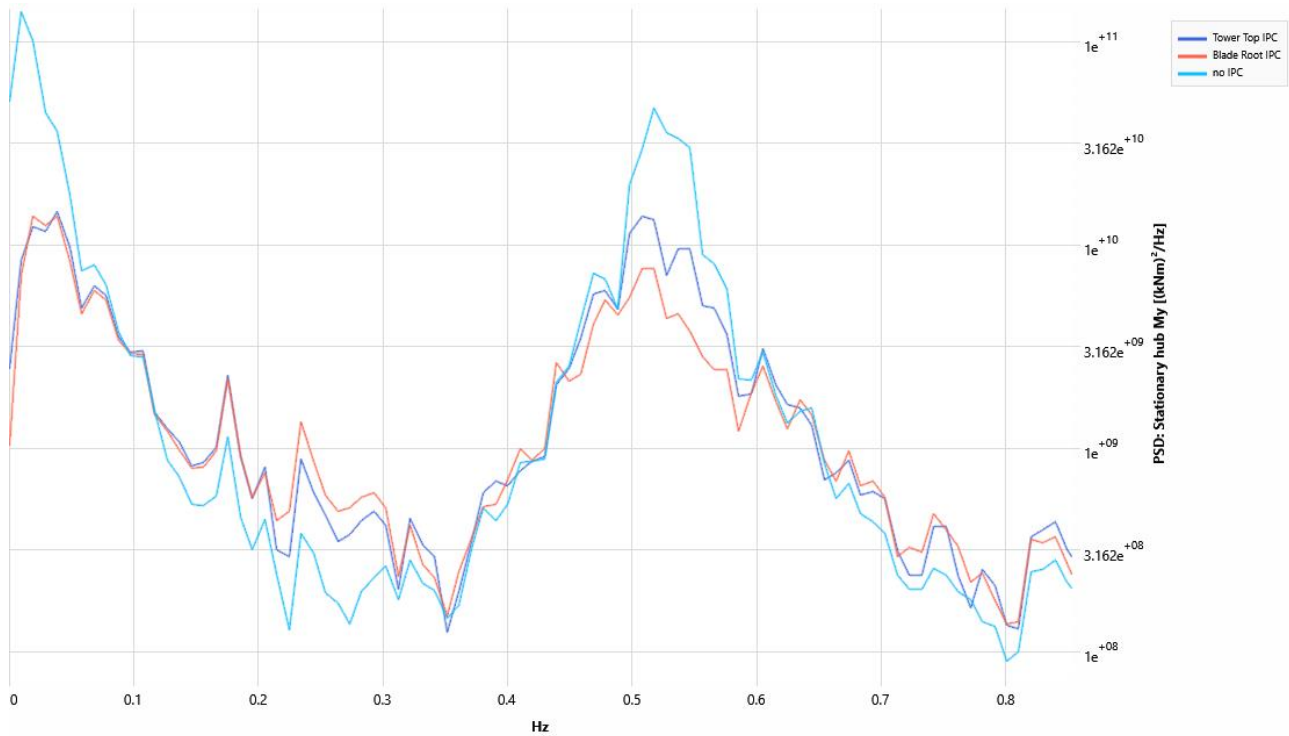


Figure 25 Stationary Hub My with 2P IPC.

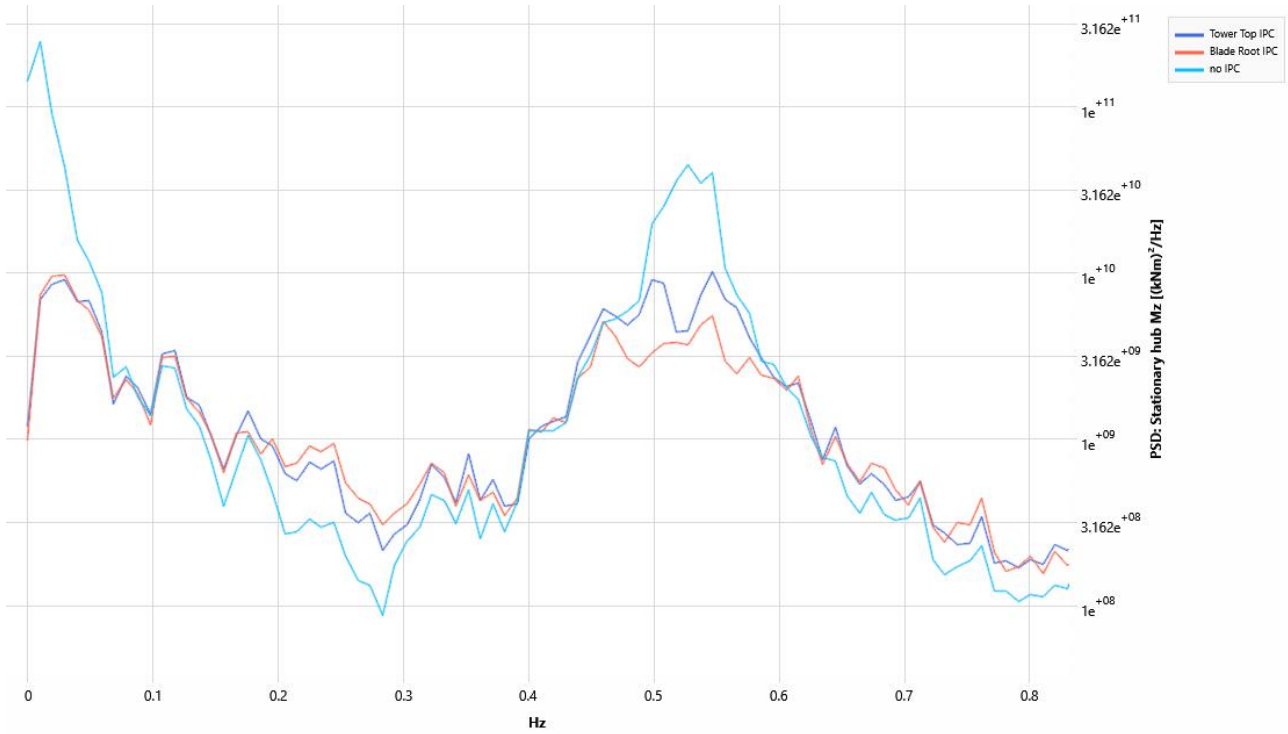


Figure 26 Stationary Hub Mz with 2P IPC.

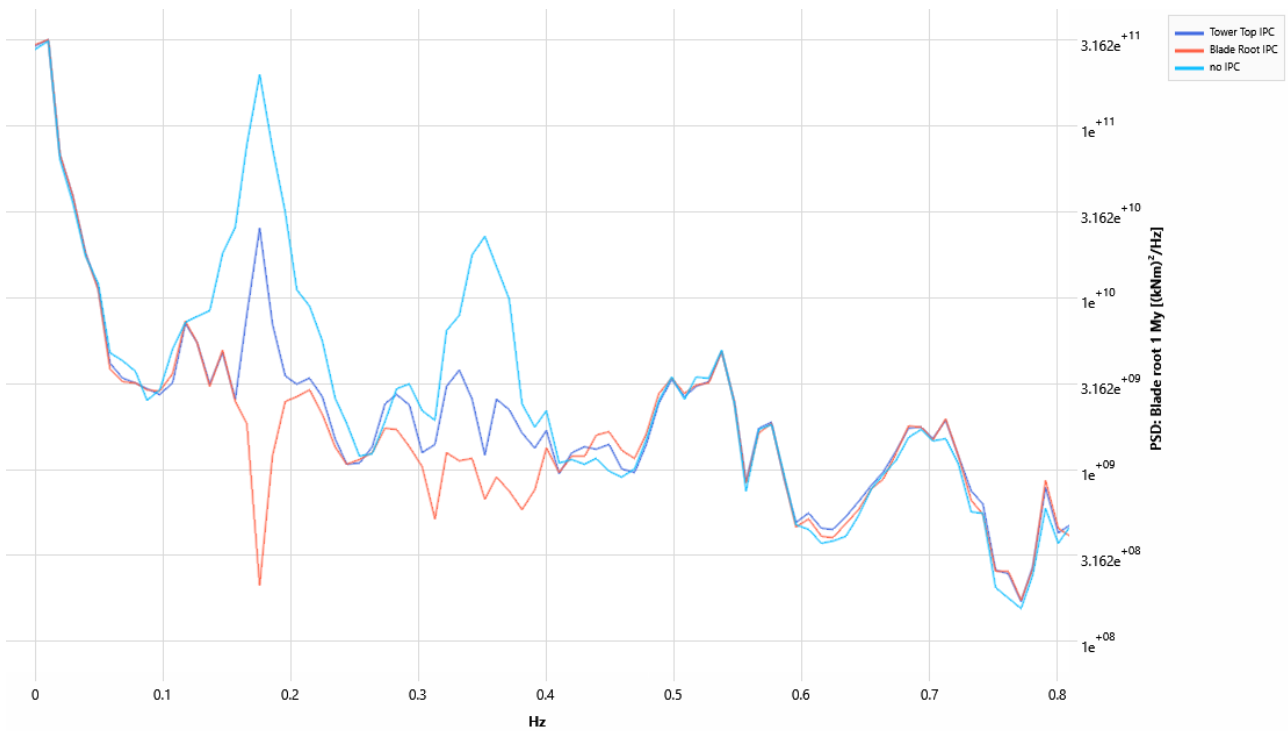


Figure 27 Effect on Blade Root My of 2P IPC. Tower top sensors (blue) and blade root sensors (orange)



Figure 28 Effect on Blade 1 pitch angle of 2P IPC. Blade root sensors (orange) and tower top sensors (blue)

2.3.2. FATIGUE LOADS (DEL) RESULTS

In the case of 2P IPC, both BR IPC and TT IPC provide significantly lower loads compared to just 1P IPC. However, for all components considered, BR IPC consistently outperforms TT IPC across all wind speeds.

At the Blade root (Figure 29, Figure 30) and yaw bearing (Figure 33, Figure 34), the difference is consistently around 3-5%, while at the Hub, the relative difference can reach 7%.

The backward and forward transformation for 2P TT IPC compounds the estimate errors in the signals, which in turn results in a drop in performance. By improving the algorithm to recreate hub loading from tower sensors, it might be possible to bring the performance closer to that of 2P BR IPC.

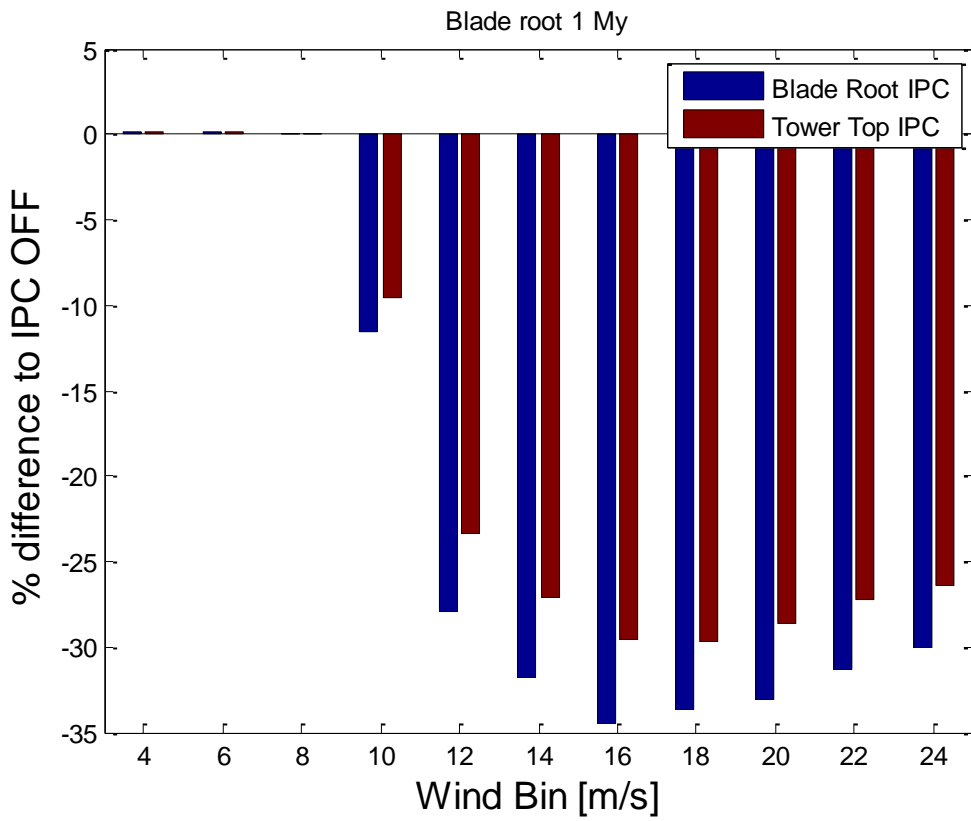


Figure 29 Relative change in blade 1 root My DEL (m=4)

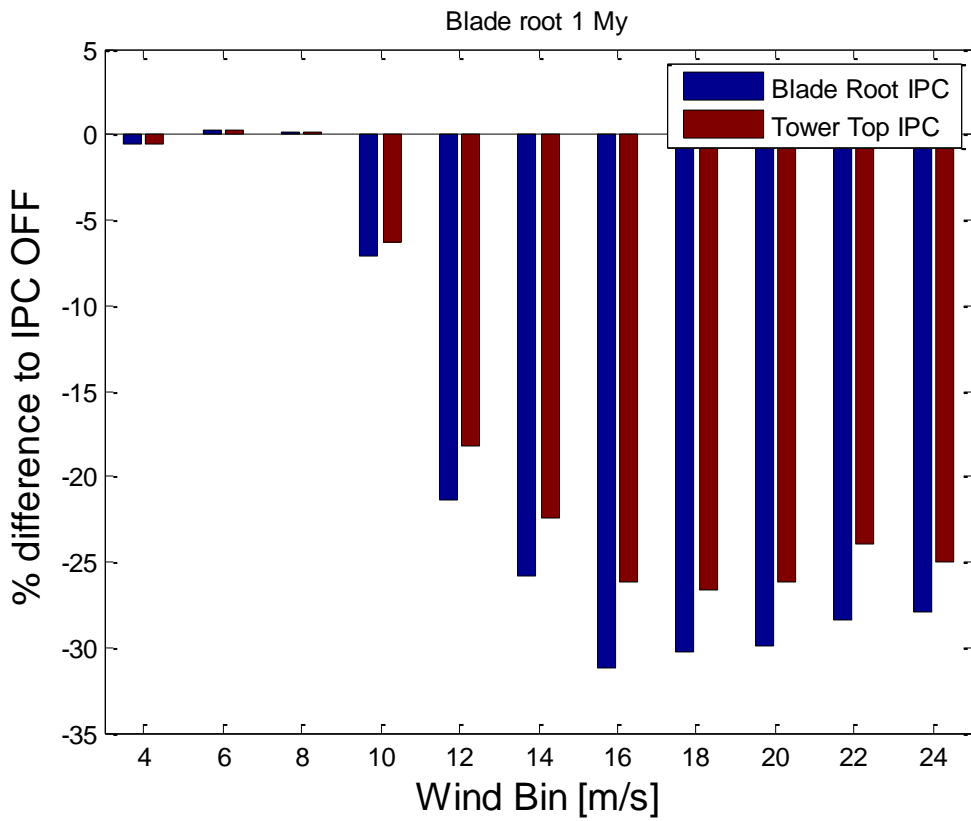


Figure 30 Relative change in blade 1 root My DEL (m=10)

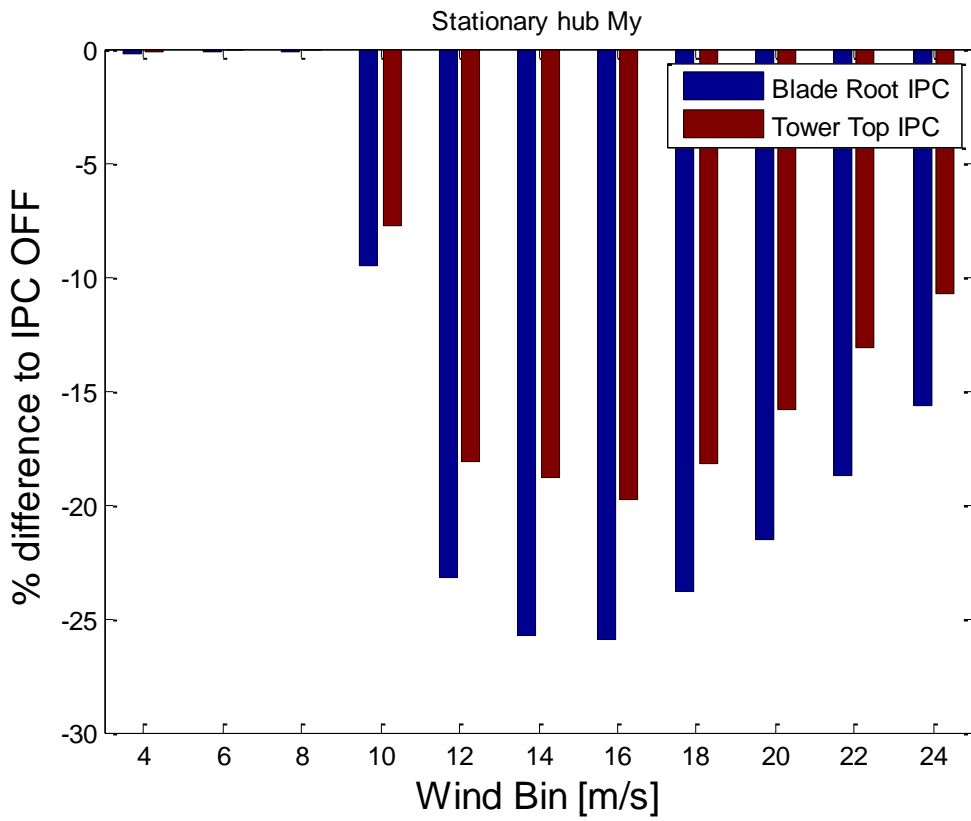


Figure 31 Relative change in Stationary Hub My DEL (m=4)

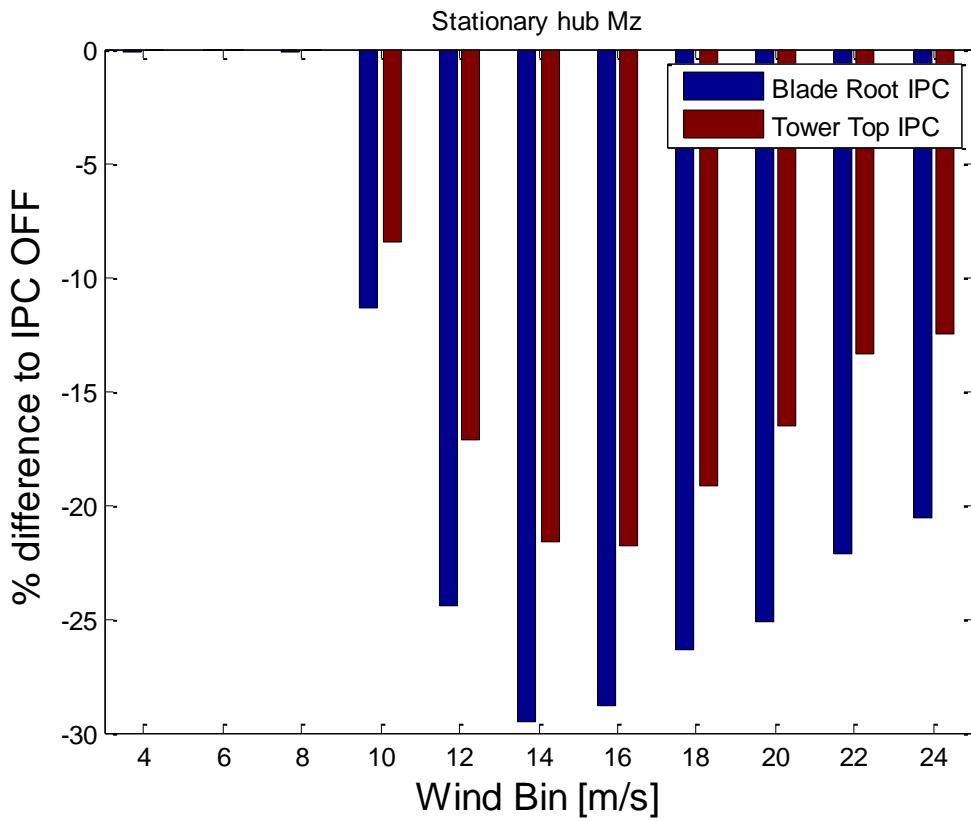


Figure 32 Relative change in Stationary Hub Mz DEL (m=4)

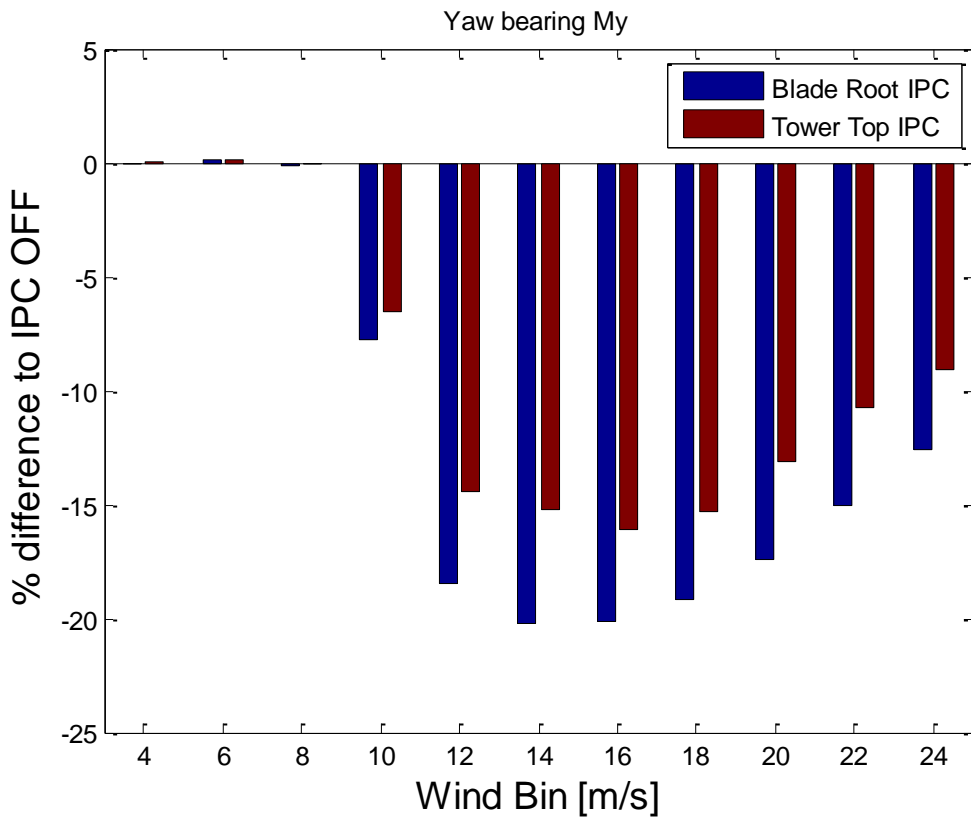


Figure 33 Relative change in Yaw Bearing My DEL (m=4)

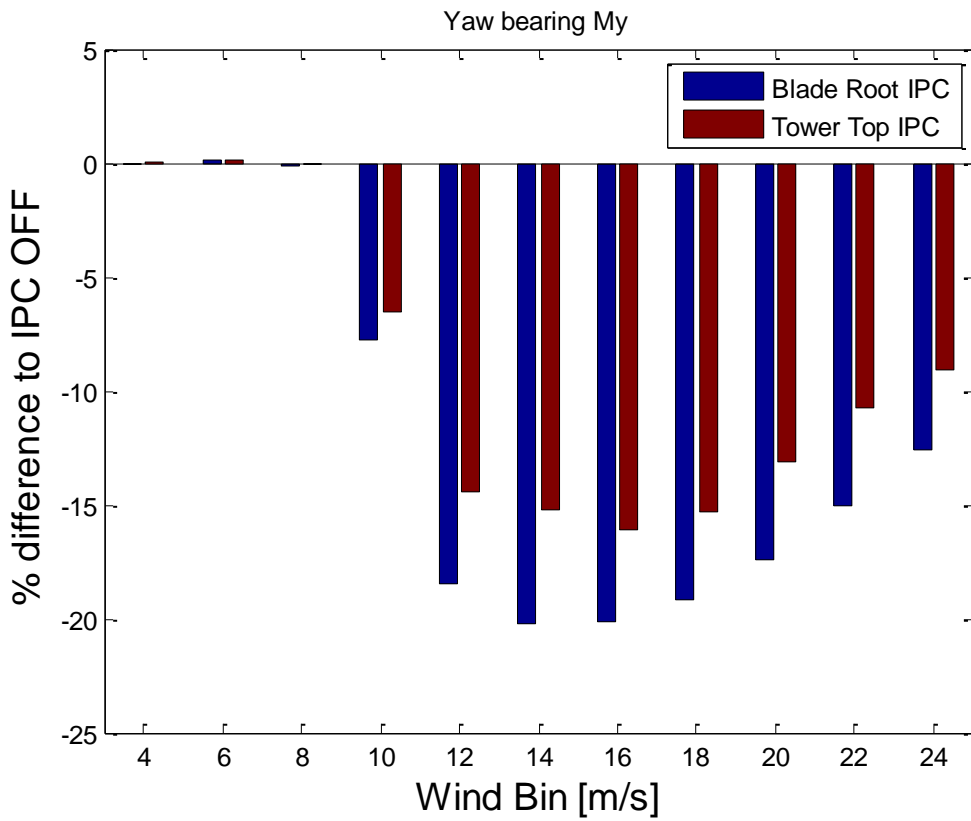


Figure 34 Relative change in Yaw Bearing Mz DEL (m=4)

3. CONCLUSIONS

Two advanced strategies for load reduction have been implemented in the controller of the Samsung 7MW Levenmouth turbine.

Lidar Assisted Control has been implemented in the form of a feed forward loop added to the Collective pitch controller of the turbine. High fidelity simulations have been run in *Bladed* to tune the LAC controller to have a similar performance in generator speed regulation as the baseline.

The controller was initially tuned using Taylor's Frozen Turbulence assumption, and then tested against a more realistic wind model that allows evolving turbulence. The results show a good fatigue loading reduction at tower base (5.7%) and blade root (3.7%) while keeping similar levels of generator speed standard deviation.

In simulations, the maximum generator overpeed was higher with the LAC controller than the baseline, but still within the overspeed alarm threshold. Nonetheless, maximum generator speed should be closely monitored during the field tests, and if needed the controller may need adjustment.

A 1P IPC control loop with tower top sensors was tuned to have similar performance as blade root 1P IPC, and the simulations results show very comparable levels of load reduction at stationary hub and blade root, with the Tower top method actually performing slightly better.

2P IPC was not originally part of the 7MW turbine controller, so it was designed and added for both IPC strategies. A 2P IPC amplitude of 1 deg was found to be the best compromise between load reduction and increased pitch activity. The load reduction shows significant improvements over the 1P IPC case for both strategies, but the blade root IPC shows a greater reduction across all wind speeds compared to the tower top IPC. The reason for this is likely due to the estimation uncertainties involved with deriving the tower top IPC signals, and in particular the estimation of the thrust.

To decide whether field testing of 2P IPC is feasible, the predicted increase in pitch activity should be considered, given that the pitch actuators were specified only for 1P IPC. The maximum pitch amplitude of 2P IPC should be increased gradually from zero while monitoring the actuators. The controller alarms defined in the supervisory controller will need to be re-tuned to accommodate the field tests when 2P IPC is being tested, but it should be kept in mind that the design is only based on DLC 1.2, since running a full set of load cases was beyond the scope of this work.

4. REFERENCES

- [1] Bladed Theory Manual
- [2] Mikkelsen T, Angelou N, Hansen K, Sjøholm M, Harris M, Slinger C, Hadley P, Scullion R, Ellis G and Vives G 2013 Wind Energy 16 625-643 ISSN 1099-1824 URL <http://dx.doi.org/10.1002/we.1564>
- [3] Bossanyi, Ervin: 'Un-freezing the turbulence: application to LiDAR-assisted wind turbine control', IET Renewable Power Generation, 2013, 7, (4), p. 321-329, DOI: 10.1049/iet-rpg.2012.0260 IET Digital Library, <https://digital-library.theiet.org/content/journals/10.1049/iet-rpg.2012.0260>
- [4] Kumar, Avishek & Hugues-Salas, O & Savini, B & Keogh, W. (2016). Tower Based Load Measurements for Individual Pitch Control and Tower Damping of Wind Turbines. Journal of Physics: Conference Series. 753. 052024. 10.1088/1742-6596/753/5/052024.
- [5] Bossanyi E A 2003 Wind Energy 6 119-128
- [6] Kumar A A, Bossanyi E, Scholbrock A K, Fleming P A and Boquet M 2015 EWEA (Paris)